



106
915
THS



This is to certify that the

thesis entitled

Characterization of the Interphase and its
Influence on the Behavior of Glass
Fiber-Reinforced Epoxy Composites

presented by

Edward Kent Drown

has been accepted towards fulfillment
of the requirements for

M.S. degree in Chemical Engineering

Lawrence T. Dwyer
Major professor

Date 8/9/91



PLACE IN RETURN BOX to remove this checkout from your record.
TO AVOID FINES return on or before date due.

DATE DUE	DATE DUE	DATE DUE
_____	_____	_____
_____	_____	_____
_____	_____	_____
_____	_____	_____
_____	_____	_____
_____	_____	_____
_____	_____	_____

MSU Is An Affirmative Action/Equal Opportunity Institution

CHARACTERIZATION OF THE INTERPHASE AND ITS INFLUENCE ON THE
BEHAVIOR OF GLASS FIBER-REINFORCED EPOXY COMPOSITES

By

Edward Kent Drown

A THESIS

Submitted to
Michigan State University
in partial fulfillment of the requirements
for the degree of

MASTER OF SCIENCE

Department of Chemical Engineering

1991

1889-007
68877

ABSTRACT

CHARACTERIZATION OF THE INTERPHASE AND ITS INFLUENCE ON THE BEHAVIOR OF GLASS FIBER-REINFORCED EPOXY COMPOSITES

By

Edward Kent Drown

Research was conducted to determine to what degree an epoxy-compatible glass-fiber sizing system alters fiber-matrix adhesion and its effect on the mechanical properties of a glass fiber-reinforced epoxy-matrix composite. Blends of the sizing system and bulk matrix were used to model the fiber-matrix interphase formed when the sizing system interacts with the matrix during fabrication of the composite. In this case, the sizing system's interaction with the matrix produced a material with an increased modulus and tensile strength but lower toughness and glass transition temperature. The presence of the sizing system increased the level of fiber-matrix adhesion and shifted the failure locus from the interface to the matrix. Mechanical testing of the composite revealed that the presence of the sizing system affects the failure behavior of interphase insensitive tests and affects both the failure behavior and properties of interphase sensitive tests.

TABLE OF CONTENTS

LIST OF TABLES	v
LIST OF FIGURES	vi
CHAPTER 1 <u>INTRODUCTION</u>	
1.1 <u>INTRODUCTION</u>	1
1.2 <u>BACKGROUND</u>	2
1.2.1 GLASS FIBERS	2
1.2.2 SILANE COUPLING AGENTS	2
1.2.3 GLASS FIBER SIZING SYSTEMS	4
1.2.4 ADHESION AT THE FIBER-MATRIX INTERFACE	5
1.3 <u>RESEARCH OBJECTIVE</u>	8
CHAPTER 2 <u>EXPERIMENTAL PROCEDURE</u>	
2.1 <u>INTRODUCTION</u>	9
2.2 <u>MATERIALS</u>	9
2.2.1 SYSTEM CONSTITUENTS	9
2.2.2 COMPOSITE FABRICATION	10
2.2.3 LAMINATE CHARACTERIZATION	11
2.3 <u>FIBER TENSILE STRENGTH</u>	14
2.4 <u>BLEND MECHANICAL PROPERTIES</u>	15
2.4.1 DYNAMIC MECHANICAL ANALYSIS	15
2.4.2 TENSILE TESTING	16
2.5 <u>INTERFACIAL CHARACTERIZATION</u>	16
2.5.1 EMBEDDED SINGLE FIBER TEST	16
2.5.2 INTERFACIAL TESTING SYSTEM	19
2.6 <u>COMPOSITE MECHANICAL PROPERTIES</u>	23
2.6.1 SHORT BEAM SHEAR TESTING	23
2.6.2 FLEXURE TESTING	23
2.6.3 TENSILE TESTING	24
2.7 <u>FRACTOGRAPHY</u>	24
CHAPTER 3 <u>RESULTS and DISCUSSION</u>	
3.1 <u>INTRODUCTION</u>	25
3.2 <u>EFFECT OF THE SIZING ON FIBER TENSILE</u>	

	<u>STRENGTH</u>	25
3.3	<u>BLEND PHYSICAL PROPERTIES</u>	27
	3.3.1 GLASS TRANSITION TEMPERATURE	27
	3.3.2 MECHANICAL PROPERTIES	28
3.4	<u>EFFECT OF THE SIZING ON INTERFACIAL</u>	
	<u>BEHAVIOR</u>	31
	3.4.1 FIBER-MATRIX FAILURE LOCUS	31
	3.4.2 FIBER-MATRIX ADHESION	35
3.5	<u>EFFECT OF THE SIZING ON COMPOSITE</u>	
	<u>PROPERTIES</u>	37
	3.5.1 SHORT BEAM SHEAR	37
	3.5.2 90° FLEXURE	38
	3.5.3 0° FLEXURE	39
	3.5.4 90° TENSILE	43
	3.5.5 0° TENSILE	43
3.6	<u>EFFECT OF THE SIZING ON COMPOSITE</u>	
	<u>FRACTOGRAPHY</u>	44
	3.6.1 SHORT BEAM SHEAR	44
	3.6.2 0° FLEXURE	46
	3.6.3 90° TENSILE	49
	3.6.4 0° TENSILE	51
CHAPTER 4	<u>CONCLUSIONS</u>	53
	LIST OF REFERENCES	55

LIST OF TABLES

Table 1.	Elemental Composition of E-Glass Fibers at the Surface and in the Bulk	2
Table 2.	Typical Components of a Glass-Fiber Sizing System	5
Table 3.	Laminate Characteristics	14
Table 4.	ITS Specimen Polishing Protocol	22
Table 5.	Mechanical Properties of D.E.R. 383/DACH/Sizing Blends	29
Table 6.	Embedded Single Fiber Results for D.E.R. 383/ DACH/Bare E-Glass	35
Table 7.	ITS Results for D.E.R. 383/DACH/E-Glass Composites	36
Table 8.	SBS Results for D.E.R. 383/DACH/E-Glass Laminates	37
Table 9.	90° Flexural Properties of D.E.R. 383/DACH/E-Glass Laminates	38
Table 10.	0° Flexural Properties of D.E.R. 383/DACH/E-Glass Laminates	39
Table 11.	90° Tensile Properties of D.E.R. 383/DACH/E-Glass Laminates	43
Table 12.	0° Tensile Properties of D.E.R. 383/DACH/E-Glass Laminates	44

LIST OF FIGURES

Figure 1.	Structure of a Silane Coupling Agent	2
Figure 2.	Hydrolysis of a Silane Coupling Agent	3
Figure 3.	Adsorption and Reaction of a Silane Coupling Agent with Surface Silanol Groups	4
Figure 4.	Chemical Bonding Theory of Fiber-Matrix Adhesion	6
Figure 5.	Interphase Theory of Fiber-Matrix Adhesion	7
Figure 6.	Polished Laminate Cross Section	12
Figure 7.	Polished and Etched Laminate Cross Section	13
Figure 8.	ITS Microindenter and Composite Specimen	20
Figure 9.	The Interfacial Testing System	21
Figure 10.	E-Glass Fiber Strength Versus Gage Length	27
Figure 11.	T_g Versus Sizing System Concentration in D.E.R. 383/DACH	28
Figure 12.	Blend Physical Properties Versus Sizing Concentration	30
Figure 13.	Fiber Break at Low Strain, D.E.R. 383/DACH/Bare E-Glass, X67	32
Figure 14.	Fiber Break at High Strain, D.E.R. 383/DACH/Bare E-Glass, X67	33
Figure 15.	Fiber Break at Low Strain, D.E.R. 383/DACH/Sized E-Glass, X67	34
Figure 16.	0° Flexure Specimens, Tensile Side, D.E.R. 383/ DACH/Bare E-Glass	40
Figure 17.	0° Flexure Specimens, Edge View, D.E.R. 383/ DACH/Bare E-Glass	40
Figure 18.	0° Flexure Specimens, Tensile Side, D.E.R. 383/ DACH/Sized E-Glass	41
Figure 19.	0° Flexure Specimens, Edge View, D.E.R. 383/ DACH/Bare E-Glass	42
Figure 20.	SBS Failure Surface, D.E.R. 383/DACH/Bare E-Glass	45
Figure 21.	SBS Failure Surface, D.E.R. 383/DACH/Sized E-Glass	46
Figure 22.	0° Flexure Failure Surface, D.E.R. 383/DACH/Bare E-Glass	47
Figure 23.	0° Flexure Failure Surface, D.E.R. 383/DACH/Sized E-Glass	48
Figure 24.	0° Flexure Failure Surface, Compressive Side, D.E.R. 383/DACH/Sized E-Glass	48

Figure 25.	0° Flexure Failure Surface, Tensile Side, D.E.R. 383/ DACH/Sized E-Glass	49
Figure 26.	90° Tensile Failure Surface, D.E.R. 383/DACH/Bare E-Glass	50
Figure 27.	90° Tensile Failure Surface, D.E.R. 383/DACH/Sized E-Glass	50
Figure 28.	0° Tensile Failure Surface, D.E.R. 383/DACH/Bare E-Glass	52
Figure 29.	0° Tensile Failure Surface, D.E.R. 383/DACH/Sized E-Glass	52

CHAPTER 1

INTRODUCTION

1.1 INTRODUCTION

Glass fiber-reinforced polymer matrix composites have been in continuous use for over forty years largely because of the development of silane coupling agents. These coupling agents are incorporated into protective coatings for glass fiber surfaces called "sizes" which contain silane coupling agents as well as processing aids. These sizes are applied to the surface of the glass fibers shortly after fiber manufacture and before composite fabrication. These sizes increase the level of adhesion between the matrix polymer and glass reinforcement and aid in the long-term retention of composite mechanical properties. While the chemistry of silane coupling agents and their interactions with both the glass fiber's surface and the polymer matrix has been extensively studied,¹⁻¹¹ little fundamental information of a predictive nature attesting to the relationships between sizing application and composite mechanical properties has been published. Contemporary art views the application of a size as necessary for ease of processing and for acceptable retention of fiber strength during handling and composite fabrication. This study was undertaken to investigate the glass fiber-sizing system-polymer matrix interphase to better understand the role of the interphase in the performance of glass fiber-reinforced epoxy-matrix composites.

1.2 BACKGROUND

1.2.1 GLASS FIBERS. The glass fibers used as reinforcements are complex mixtures of oxides, a typical elemental composition for E-glass fibers in the bulk and at the surface is given in **Table 1**.

Table 1. Elemental Composition of E-Glass Fibers at the Surface and in the Bulk¹

Location	B	Ca	O	F	Mg	Al	Si
Bulk	4.5	6.4	61.8	0.3	2.3	5.8	18.8
Surface	3.4	1.9	61.2	1.4	0.6	7.0	24.3

The oxide groups present on the fiber surface react readily with atmospheric water to form hydroxyl groups of the type M-OH where M = silicon or aluminum.²

1.2.2 SILANE COUPLING AGENTS. The structure of a typical silane coupling agent is shown in **Figure 1**.

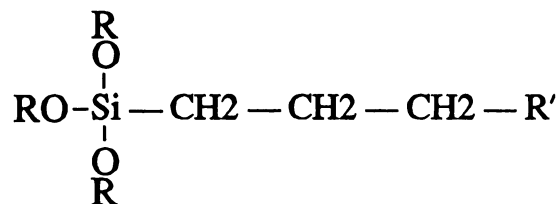


Figure 1. Structure of a Silane Coupling Agent

The coupling agent consists of a central silicon atom connected to an organofunctional group (R') via a propyl chain. Three methoxy or ethoxy groups (OR) are also attached to the silicon atom. The organofunctional group can be selected to be reactive with the matrix, in the case of epoxy, R' can be an epoxide group or a functional group found in

the hardener. Before being applied to the fibers, the coupling agent is converted to the silanol form by hydrolysis, shown in **Figure 2**.

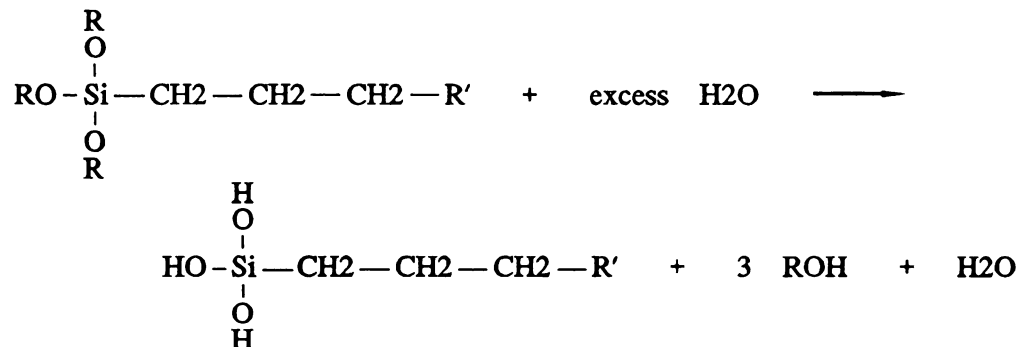
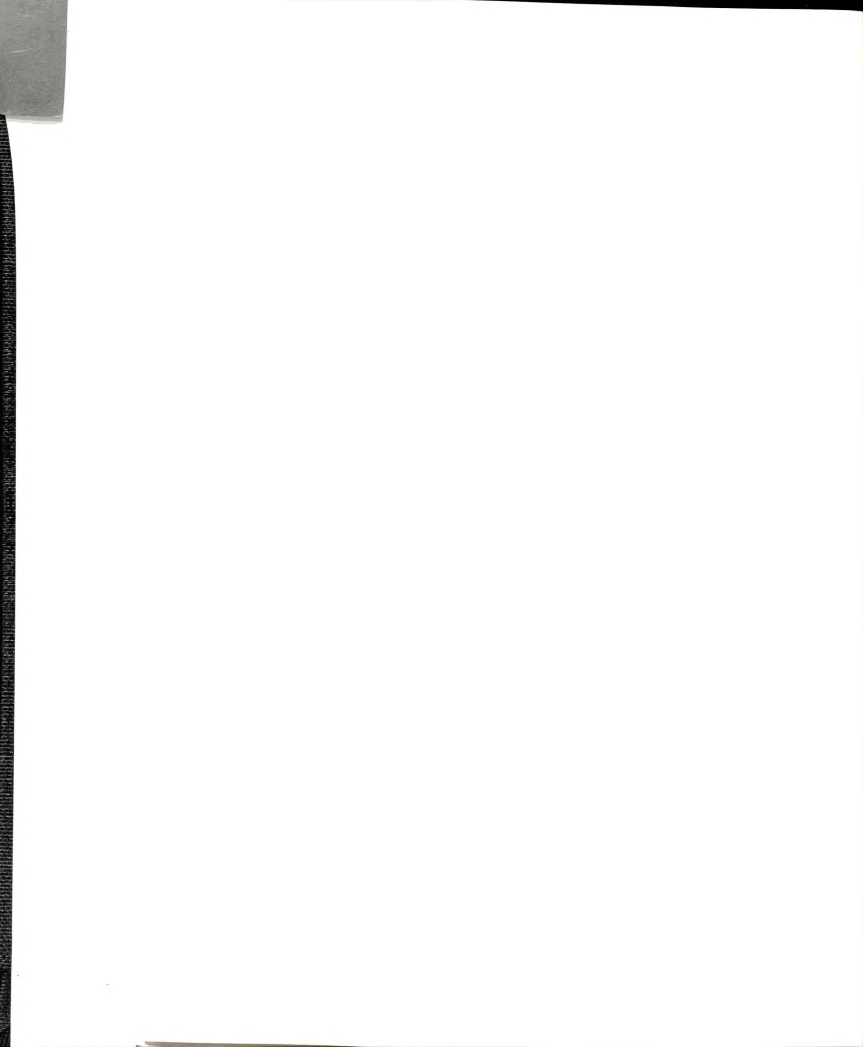


Figure 2. Hydrolysis of a Silane Coupling Agent

The hydrolyzed form of the coupling agent can then undergo further elimination reactions between silanol groups to form oligomers and a three dimensional polysiloxane network.^{3,4}

The structure of physisorbed and chemisorbed silane coupling agents at silica (SiO_2) and glass surfaces has been investigated via FTIR,⁵ NMR,^{6,7} and XPS.⁸ The adsorption and reaction of silane coupling agents with the fiber surface, illustrated in **Figure 3**, is a multistep process. The coupling agent physisorbs onto the fiber surface through hydrogen bonding of the hydroxyl groups on the coupling agent and fiber surface. The coupling agents have been found to then form covalent oxane bonds via an elimination reaction between a silanol group on the silane coupling agent and a hydroxyl group on the glass surface.⁹ Silane coupling agents also form oligomers in solution and may adsorb as such. This interaction extends beyond the monolayer range and evidence indicates that the silane coupling agent adsorbs in multilayers when possible.^{10,11}



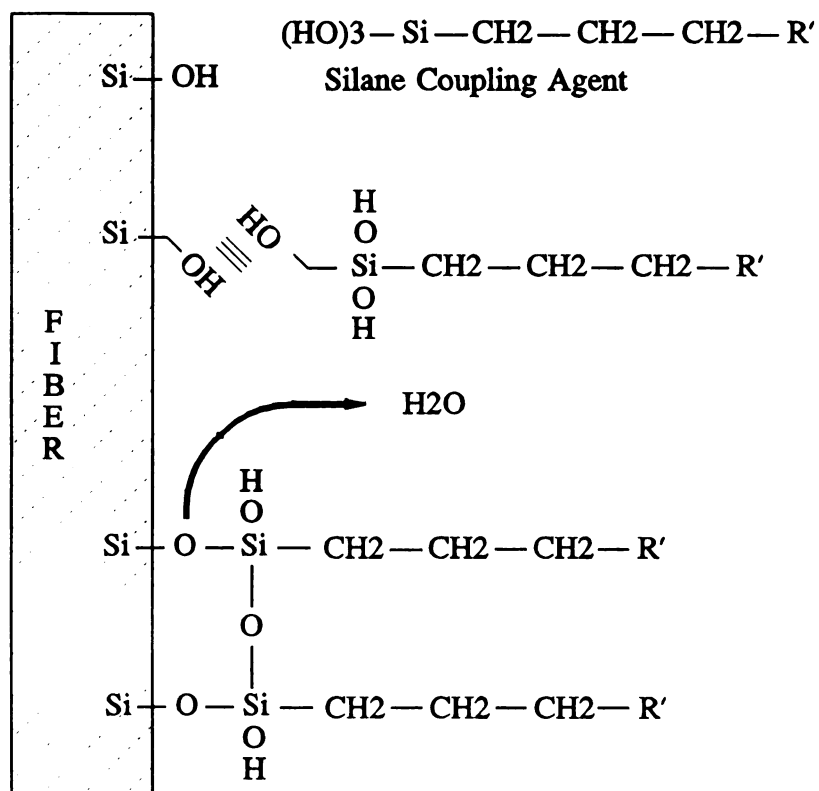


Figure 3. Adsorption and Reaction of a Silane Coupling Agent with Surface Silanol Groups

1.2.3 GLASS FIBER SIZING SYSTEMS. The composition of a glass-fiber sizing system is complex, with the coupling agent comprising a relatively small portion of the material applied to the fibers. Most commercial sizing systems, especially those used in glass fiber-reinforced epoxy composites are complex proprietary compositions. For example, **Table 2** lists the general proportion of components in a commercial sizing system excluding the solvent or carrier used to apply the mixture. The film-forming resin aids in the distribution of the sizing over the fibers and acts as a binder providing integrity to the fiber tow. Antistatic agents prevent the build-up of static electricity during handling. Lubricants decrease friction between the fibers, thereby reducing

Table 2. Typical Components of a Glass-Fiber Sizing System¹²

Component	Percent
Film-Forming Resin	1 ~ 5
Antistatic Agent	0.1 ~ 0.2
Lubricant	0.1 ~ 0.2
Coupling Agent	0.1 ~ 0.5

abrasive damage. The remaining fraction of the sizing system is the silane coupling agent, the optimum amount has been found to be 10 to 20 monolayer equivalents on the surface.¹³

The constituents of typical sizing systems are compatible and can interact with each other. The resulting distribution of these components in the interphase region is not well understood, with the formulation of effective sizing systems being an empirical undertaking for the most part. The processing aids may change the interphase properties in a manner similar or counter to that of the silane coupling agent acting alone.

1.2.4 ADHESION AT THE FIBER-MATRIX INTERFACE. The two most common concepts of adhesion across the fiber-matrix interface are the chemical bonding and interphase theories. The chemical bonding theory, **Figure 4**, holds that approximately a monolayer of the silane coupling agent acts as a bridge between the glass surface and the polymeric matrix. The presence of covalent bonding between the coupling agent and the fiber surface has bolstered the chemical bonding concept. However, chemical bonding cannot account for the increase in adhesion experienced between non-reactive matrices such as polyolefins and silane coupling agent-treated inorganic reinforcements



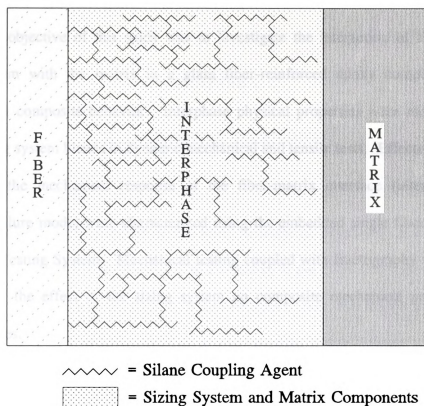


Figure 5. Interphase Theory of Fiber-Matrix Adhesion

silane coupling agents. The increased hydrolytic stability of coupling agent treated composites likewise has been proposed to occur through hydrolyzable bonds between the silane coupling agent and reinforcement surface that can break and reform easily enough to relieve stress at the interface and preserve the integrity of the composite. This type of argument is supported by an interphase model¹⁷ in which the molecular structure of the interphase is most often considered to be an interpenetrating network between the coupling agent and matrix resin.

1.3 RESEARCH OBJECTIVE

The objective of this study was to investigate the interaction of a commercial sizing system with the matrix in a glass fiber-reinforced epoxy composite and its influence on composite behavior. Interphase physical properties were modelled using epoxy/sizing system blends in dynamic mechanical and tensile tests. Effects of the sizing system on the mechanical response of the fiber-matrix interface (interfacial shear strength, failure mode) were characterized using the embedded single fiber test and the Interfacial Testing System. Mechanical testing coupled with fractography were used to characterize the effect of the sizing system on composite mechanical properties and failure modes.

CHAPTER 2

EXPERIMENTAL PROCEDURE

2.1 INTRODUCTION

The experimental program of this study focussed on developing an understanding of how a commercial sizing interacts with the matrix in the glass fiber-matrix interphase and its effect on composite properties. Measurements of the glass transition temperature and tensile properties of bulk samples of epoxy/sizing system blends were made to evaluate the range of properties of expected interphases. The mechanical response of the fiber-matrix interphase (interfacial shear strength and failure mode) was evaluated using the embedded single fiber method and the Interfacial Testing System. Composite mechanical properties were measured (short beam shear, 0° and 90° flexure, 0° and 90° tension) and fractography conducted on unidirectional laminates.

2.2 MATERIALS

2.2.1 SYSTEM CONSTITUENTS. A typical epoxy matrix, a commercial sizing system and E-glass reinforcing fibers were selected as the materials to be used in this study. A diglycidyl ether of bisphenol A based resin, D.E.R. 383[®] (*Dow Chemical Company*), was selected as the epoxy resin. 1,2-Diaminocyclohexane (DACH) (*Aldrich Chemical Company*) was used as the hardener at 15.6 parts per hundred of resin by weight. E-

glass tows (1600 filaments/tow, 13 μm nominal filament diameter) were supplied by the *Pittsburgh Plate Glass Company* (PPG). The fibers were supplied with two surface treatments, the first being deionized water only and the second a commercial epoxy-compatible sizing system. The water-treated fibers are referred to as "bare" and the fibers coated with the size are referred to as "sized". The sizing system was also supplied in bulk form for the preparation of epoxy/size blend samples which were used for mechanical property measurements.

2.2.2 COMPOSITE FABRICATION. Unidirectional laminates were prepared for single fiber microindentation measurements with the Interfacial Testing System (ITS) and for short beam shear, flexure and tensile mechanical testing. A filament winding prepregger was used to prepare glass/epoxy prepreg tapes. The glass fiber tow was supplied on a cardboard core and stored in a polyethylene bag to prevent drying out of the tow. The core was mounted on a frame and axle to allow the unwinding of the tow from the outside of the package. The tow passed through a drying oven held at 110 °C with a residence time of about 5 seconds. The tow then entered the resin pot where it travelled between 3 polished stainless steel pins that helped separate the filaments and aid impregnation of the resin into the tow. The tow exited the resin pot through a slit die of dimensions 0.20 x 1.8 mm. The impregnated tow was guided by a roller and laid onto a rotating drum. The drum was covered with a layer of release film. The resin pot, guide pins and rollers were held at room temperature with the process requiring about 2 hours to produce a tape 11 inches wide and 6 feet long. The tapes were cut into 12 inch lengths and stacked to produce unidirectional laminates of 12 or 18 plies. The

uncured laminates were placed between 1/2 inch thick aluminum caul plates that were covered with 2 plies of bleeder cloth and 1 ply of porous Teflon® (*DuPont*) coated glass release fabric. Self-adhesive cork dams surrounding the prepreg prevented its escape from between the caul plates during processing.

The temperature cycle used to cure the laminates was 16 hours at room temperature, 2 hours at 80°C and 2 hours at 175°C with 5°C/min ramps between soaks. Directly after lay-up, the caul plate-laminate assembly was placed in a Carver Laboratory Press and sufficient load applied to produce 0.7 MPa (100 psig) in the laminate. This load was maintained for 30 minutes in order to bleed-out excess resin. The assembly was then placed in a vacuum bag and loaded into an autoclave for the elevated temperature portion of the cure cycle. A pressure of 0.9 MPa (125 psig) was applied to outside of the vacuum bag assembly for the duration of the autoclaving. Vacuum of -0.09 MPa (-28 in Hg) was applied for the first 30 minutes of the 80°C soak period and vented to atmosphere for the remainder of the cure cycle.

2.2.3 LAMINATE CHARACTERIZATION. Laminate quality was assessed after fabrication through the use of Optic Numeric Volume Fraction Analysis¹⁸ (ONVFA), a technique which allows quantitative assessment of fiber volume fraction using optical methods. The procedure requires the preparation of a composite cross section for observation with a reflected light microscope, digitizing a video image of the specimen and then counting the fibers in a defined area of the cross section. One other variable, the area per fiber, is obtained from manufacturer's lot data or determined from the fiber tow directly. The fiber volume fraction is then determined from (1):

$$\text{Volume Fraction Fibers} = \text{Fibers per Image} * \frac{\text{Area per Fiber}}{\text{Area per Image}} \quad (1)$$

For this study, three randomly selected sections about 2 cm x 2 cm were removed from the laminate of interest and embedded in polyester metallographic mounts with the long axis of the fibers perpendicular to the mount surface. The specimens were polished using standard metallographic methods to a 1 μm finish on a rotating lap polisher. This produced a surface with well defined fiber ends. However, as shown in **Figure 6**, the contrast between fiber and matrix was poor.

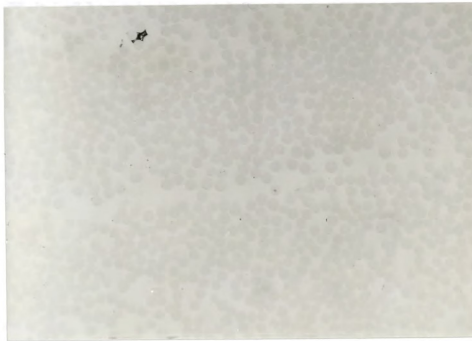


Figure 6. Polished Laminate Cross Section

ONVFA was originally developed for carbon fiber-reinforced epoxy composites which exhibited a high contrast between fiber and matrix after polishing. To increase the

contrast between fiber and matrix in the glass fiber-reinforced epoxy composites, the polished sections were etched for 5 minutes with CHROMERGE® (*VWR Scientific*), rinsed with deionized water for 10 minutes in an ultrasonic bath and dried with compressed air. As shown in **Figure 7**, this treatment retained the profile of the fiber ends while the loss of matrix has increased the contrast to allow accurate counting of the fiber ends.

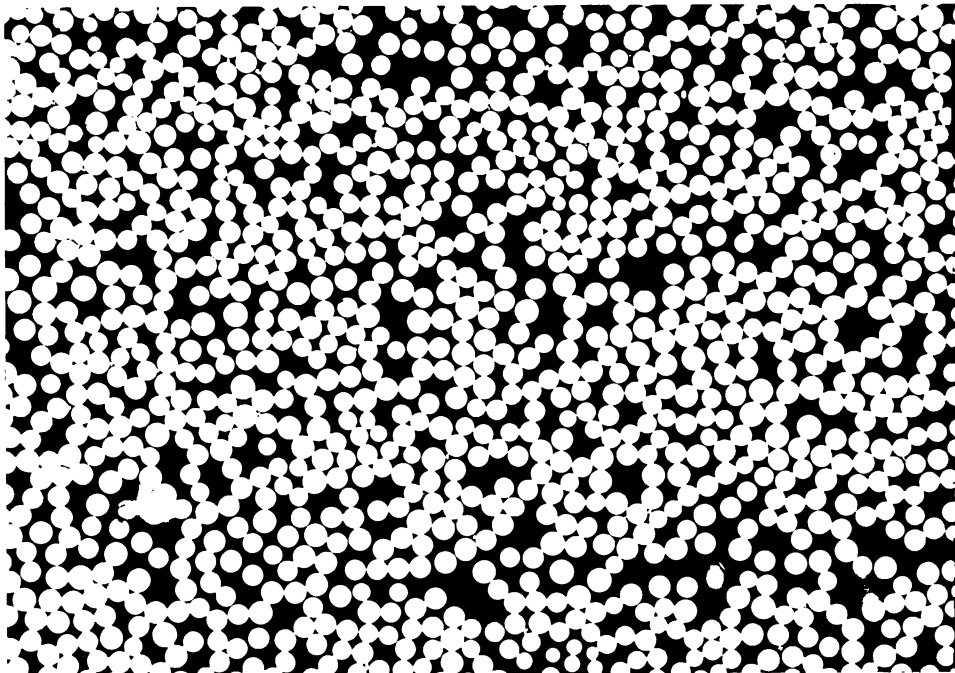


Figure 7. Polished and Etched Laminate Cross Section

The specimen was mounted on a metal slide and adjusted to give uniform focus across its cross section. A reflected-light image was fed to a CCD camera and captured with a frame-grabber for analysis. The counting parameters were adjusted to give about the same number of double counted and missed fiber ends per digitized image. Fifteen images from each cross section were digitized and the fibers counted. Measured sections

of bare fiber tow were dried at 100 °C for 2 hours and weighed to determine the average area per fiber of $125.6 \pm 1.5 \mu\text{m}^2/\text{fiber}$. The void volume fraction was determined using the measured fiber volume fraction and the density of the laminate measured gravimetrically.

Table 3. Laminate Characteristics

Laminate	Number of Plies	Fiber Type	Fiber Volume Fraction (%)	Void Volume Fraction (%)	Test Specimens
042390-1	18	Bare	63.8 ± 1.9	0.45 ± 0.39	Short Beam Shear 0° Tensile
040990-2	12	Bare	65.6 ± 1.5	0.63 ± 0.28	90° Flexure 90° Tensile
050290-2	12	Bare	63.2 ± 1.9	0.62 ± 0.37	0° Flexure
041390-2	18	Sized	65.1 ± 2.2	0.65 ± 0.45	Short Beam Shear 0° Tensile
042090-1	12	Sized	63.6 ± 1.6	0.67 ± 0.30	0° Flexure
040990-1	12	Sized	63.6 ± 2.0	0.48 ± 0.39	90° Flexure 90° Tensile

2.3 FIBER TENSILE STRENGTH

Fiber tensile strengths were measured on a test fixture specifically designed for reinforcing fibers. The apparatus consists of a sample preparation jig and a loading frame mounted on the stage of an Olympus BH-2 microscope. The jig holds two mounting blocks to provide a reproducible gage length between the blocks. A groove

machined in the top of each block keeps the fiber axis parallel with the loading axis. The fiber is secured to the blocks with 1,5-Diphenylcarbohydrazide (DPCH) (*EM Science*), which is melted with a soldering iron applied to the underside of the mounting block. The fiber is checked for alignment and to ensure that a meniscus of DPCH did not form along the gage length of fiber.

The mounting blocks are secured to a carrier for transfer to the loading frame. The blocks rest on rail-mounted supports. One block is attached to a load cell, the other to a linear motion stage. Care is taken during the mounting and loading procedures to not apply tension to the fiber. The carrier is removed and any slack is removed from the fiber. The diameter of the fiber is measured with a calibrated filar eyepiece at three points along its diameter. The output of the load cell is fed to a digital voltmeter and chart recorder to record the load at failure. Breaks that occur at the mounting blocks are rejected. Prior to testing, sections of fiber tow were dried at 80 °C for 10 minutes. Ten individual fiber strengths were obtained for each fiber type at gage lengths of 25.4, 10.2 and .65 mm.

2.4 BLEND MECHANICAL PROPERTIES

2.4.1 DYNAMIC MECHANICAL ANALYSIS. A DuPont model 983 DMA interfaced with a 9900 model controller was used to perform dynamic mechanical testing on the epoxy/sizing system blends. Stoichiometric mixtures of D.E.R. 383 and DACH were first prepared, then sufficient sizing system was added to produce the desired concentration on a weight percent basis. The mixture was degassed and poured into



silicone RTV-664* (*General Electric Company*) molds that contained 4 cavities 3.2 x 12.5 x 60 mm. The specimens were cured at room temperature for 16 hours in a desiccator then placed in a forced convection oven and ramped to 80°C at 5°C/min and held at that temperature for 2 hours. The samples were allowed to cool to room temperature, removed from the mold and replaced in the oven on a metal sheet for a 2 hour postcure at 175°C. The free surface of the specimens was ground on a Struers Abramin polisher using 320 grit SiC paper and water to produce parallel surfaces.

The DMA was operated in the fixed frequency mode at 1 Hz and a peak to peak amplitude of 0.6 mm. A DuPont Liquid Nitrogen Cooling Apparatus (LNCA-II) was used to achieve subambient temperatures. The temperature profile used was: a ramp to -20°C, soak for 5 minutes then ramp at 5°C/min to 220°C. Three specimens were tested for each blend.

2.4.2 TENSILE TESTING. Tensile properties of the blends were measured according to ASTM standard D638-84¹⁹ using Type I specimens which were cast in a manner identical to that used to prepare DMA test specimens. The specimens were polished to a 1 μm finish on all surfaces and stored in a desiccator until tested. Five specimens of each blend were tested on a United Testing System SFM-20.

2.5 INTERFACIAL CHARACTERIZATION

2.5.1 EMBEDDED SINGLE FIBER TEST. Two methods, the embedded single fiber test and the Interfacial Testing System (ITS) were used to examine changes in fiber-matrix adhesion and failure behavior. The embedded single fiber test uses a model



composite system consisting of a single fiber embedded in a tensile coupon of the matrix of interest.^{20,21} The coupon is placed in a jig mounted on a microscope stage that permits simultaneous tensile loading of the coupon and direct high magnification observation of the failure process of the fiber. Kelly²² first analyzed the failure of the fiber which occurs through the transfer of tensile loads on the matrix to the fiber through shear forces at the fiber-matrix interface. As the tensile loads in the matrix increase, the fiber fractures at points where flaws have reduced the fiber's tensile strength. As this population of flaws is reduced, the load required to fracture the fiber exceeds the stress that can be supported by the interface and the fiber breakage stops. Once the fiber has stopped fracturing, it is said to have reached the critical transfer length (critical length), l_c , which is a measure of the interfacial shear stress. Shear lag analysis of the specimen, assuming ideal fiber properties and uniform distribution of loads yields the relationship (2) for the interfacial shear stress, τ :

$$\tau = \left(\frac{\sigma_f}{2} \right) * \left(\frac{d_f}{l_c} \right) \quad (2)$$

where d_f = fiber diameter and σ_f = fiber strength at a gage length equal to the critical length. In practice, the measured fragment lengths are not a single value, but rather a distribution of values between $l_c/2$ and l_c . This distribution is principally due to the random population of flaws along the length of the fiber. To account for the inhomogeneities in fiber strengths, the measured fiber lengths are best fit to a two-parameter Weibull²³ distribution. This distribution is used to characterize the strength of brittle materials such as glass fibers. The modified expression (3) for the interfacial

shear strength, τ :

$$\tau = \left(\frac{\sigma_f}{2 * \beta} \right) * \Gamma \left(1 - \frac{1}{\alpha} \right) \quad (3)$$

now contains α and β , the Weibull shape and scale parameters and the gamma function, Γ . During the loading process the behavior at the fiber-matrix interface is observed. Transmitted light photomicrographs can reveal the presence of matrix or interfacial cracks at fiber breaks and other phenomena that evolve as the coupon is loaded. Epoxy matrices are stress birefringent, allowing qualitative evaluation of the stress fields at the fiber breaks through the use of crossed polarizing filters.

The single fiber embedded shear strength test specimen is a single fiber encapsulated in an epoxy tensile coupon. A silicone RTV-664* (*General Electric Company*) mold with eight cavities is used for the fabrication of the coupons. The cavities are ASTM standard tensile coupons, 60 mm long with a gage section 25.4 mm long, 4 mm wide and 1.5 mm thick. Sprue slots are molded into the end of each cavity. A single filament is removed from a fiber tow and secured in the sprue slots with hot-melt adhesive. Care is taken to ensure that no tension is applied to the filaments during separation or while they are secured in the slots. The components of the matrix are thoroughly mixed and degassed in a vacuum oven for 5 minutes at room temperature to remove air entrained during the mixing process. The molds with the single fibers are also treated in the vacuum oven. The mold is infiltrated by filling one end of a cavity and allowing the resin to flow to the other end, thereby preventing the entrapment of air bubbles in the coupon. The mold is then transferred to a desiccator for a 16 hour cure

at room temperature followed by a 5°C/min ramp to 80°C for a 2 hour soak. After the molds have cooled, the test coupons are removed, placed on an aluminum sheet, and ramped to 175°C at 5°C/min for a 2 hour postcure. The coupons are allowed to cool at 5°C/min to room temperature.

The free surface of the coupons are polished to a 1 μm finish using a Struers Abramin polisher to allow clear microscopic observation of the fracture process. Specimens are mounted in a tensile testing apparatus that permits direct observation of the fracture process via transmitted light. The specimen is strained in increments indicated on a dial gauge, at each increment the strain and number of fiber breaks is recorded. After the number of breaks has reached a plateau, the fiber fragment lengths and fiber diameter are measured with a filar eyepiece.

2.5.2 INTERFACIAL TESTING SYSTEM. The interfacial testing system (ITS) (*Schares Instrument Corporation, Houston, TX*) measures the interfacial shear strength of fibers in an actual composite,^{24,25} calculated from the load at debond of a single fiber. **Figure 8** is a schematic of the process of the test, considering only the test specimen and microindenter. The fiber of interest is loaded by the microindenter until failure at the fiber-matrix interface is detected, either by a load drop or the appearance of an interfacial crack. The result is calculated using the finite element modelling results of Tsiang²⁶ and Grande.²⁷ The model was axi-symmetric, consisting of a cylinder representing the fiber surrounded by a constant thickness of matrix material. Beyond the layer of matrix, the material properties were assumed to be those of the composite. To model continuous fibers, their lengths were chosen to be many times their diameter. The



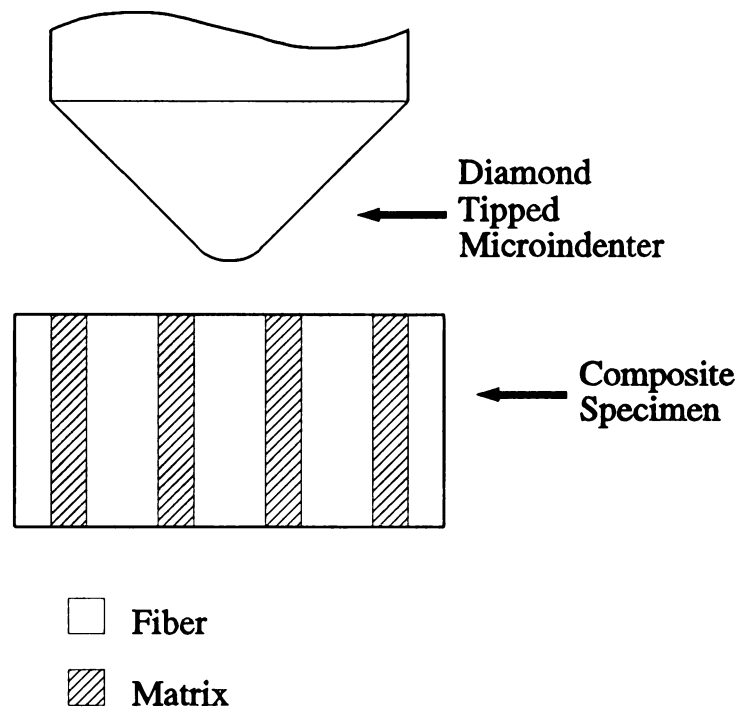


Figure 8. ITS Microindenter and Composite Specimen

load was modelled as an applied pressure to the surface of the fiber and the results did not vary appreciably with loading areas ranging from 10 to 60% of the fiber cross section. The maximum shear stress occurred 0.25 to 0.55 fiber diameters below the surface of the specimen. The maximum shear stress was considered a reasonable choice as the failure criteria as the other interfacial stresses were smaller and compressive in nature.

The ITS, shown in **Figure 9**, consists of a Mitutoyo Metallographic FS100 microscope with the stage modified to house Klinger linear motion stages for x, y and z translation with 1 μm x, y resolution and 0.04 μm resolution in the z direction. Mounted on the stages are a Sartorius L610 weighing mechanism and a specimen holder. Attached to the objective lens is a collar which holds the diamond-tipped indenter, the

profile of which is a 90° cone with an included tip radius of $10\ \mu\text{m}$. Stage controllers and the balance readout are interfaced with a Zenith 386 20MHz microcomputer for control through the software. Observation and selection of fiber ends for testing is done via a video camera and monitor.



Figure 9. The Interfacial Testing System

The specimen used for ITS testing can be any section of composite, provided that after mounting and polishing, fibers normal to the polished surface can be found. A section approximately $1\ \text{cm} \times 1\ \text{cm}$ was cut from the laminates previously prepared. The sections were embedded in $2.54\ \text{cm}$ diameter phenolic ring mounts with epoxy-based room temperature cured mounting media, oriented so that the fiber ends were normal to the face of mount to be polished. The initial steps of the polishing were accomplished on a Struers Abramin polisher and the final step on a Beuhler Vibromet I vibrating lap

polisher. The polishing used protocol is listed in **Table 4**.

Table 4. ITS Specimen Polishing Protocol

Abrasive	Lubricant	Duration
320 grit SiC	Water	0:30 min
1000 mesh SiC	Water	2:00 min
2400 mesh SiC	Water	3:00 min
4000 mesh SiC	Water	4:00 min
1 μ m diamond	Oil	30:00 min

After polishing, the specimens were stored in a desiccator until testing. Once mounted in the specimen holder, the specimen was scanned for fibers that were spaced a minimum of 2 μ m and a maximum of one-half of their diameter from the nearest neighbor. Matrix conditions near the fiber of interest also were considered. Fibers near voids, cracks, or surface damage or those fibers that showed a pre-existing interfacial crack were rejected. Once a suitable fiber end was located, its diameter and distance to nearest neighbor were entered for data reduction purposes. The fiber tensile modulus and matrix shear modulus are also required for the analysis. The fiber's coordinates are recorded directly from the stage controllers to the computer. The operator begins the test from the keyboard. The x,y stages move the fiber end to a position directly under the tip of the indenter, the z stage then moves the sample surface to within 4 μ m of the tip. The z stage approach is slowed down to 0.04 μ m/step at a rate of 6 steps/second. The balance readout is monitored, at a load of 2 grams the loading is stopped and the fiber end returned to the field of view of the camera. The location of the indent is noted and corrections are made

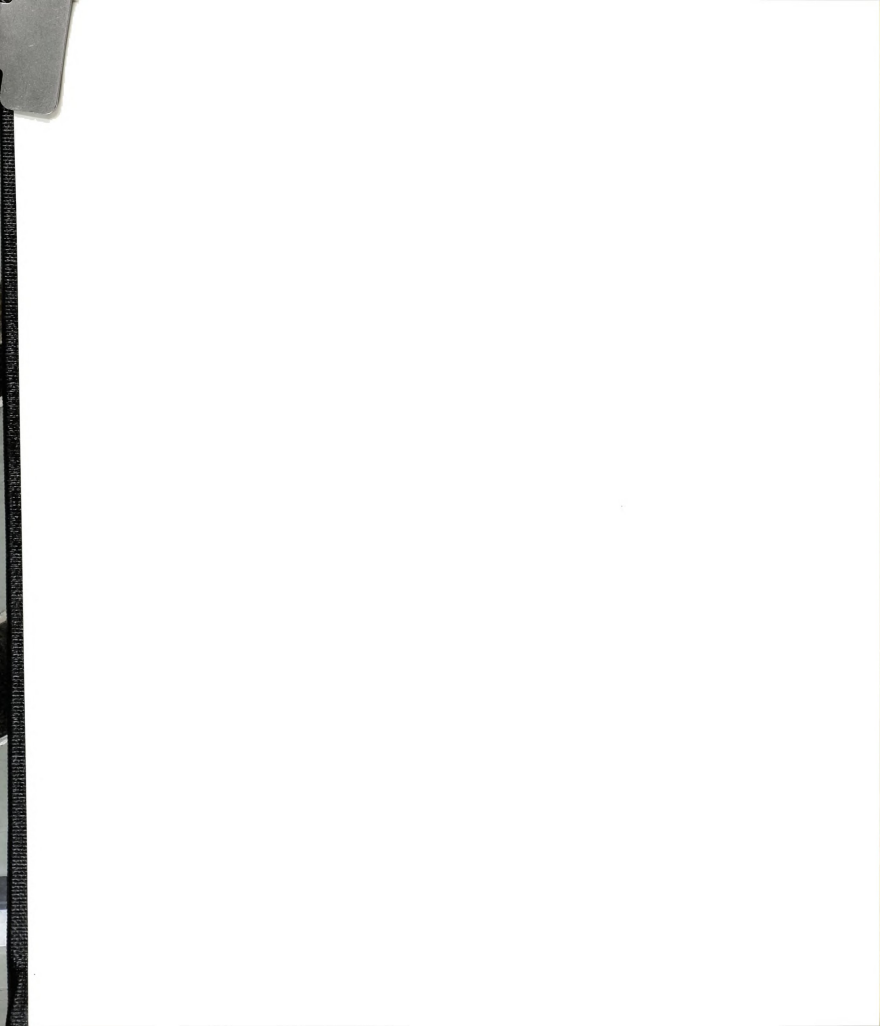


if necessary to center the point of contact. Loading alternating with observation of the fiber-matrix interface is then continued from 4 grams in approximately 1 gram increments. Debond is determined to have occurred when an interfacial crack is visible for 90 to 120 degrees on the fiber perimeter. The load at which this occurs is used to calculate the interfacial shear strength.

2.6 COMPOSITE MECHANICAL PROPERTIES

2.6.1 SHORT BEAM SHEAR TESTING. Short beam shear tests (ASTM D2344-84) were conducted on 18 ply unidirectional laminates. Specimens were cut from laminates using a water-cooled diamond saw. The support-span-to-thickness ratio used was 5 to 1 with a corresponding specimen-length-to-thickness ratio of 7 to 1. The specimen width was fixed at 6.4 mm. The specimen was three point loaded, the two end supports were set to the span previously determined and the load was applied to the midpoint via a loading nose. The crosshead speed was 1.3 mm/min. The load at break was recorded along with the failure mode, i.e. shear or tensile failure. All composite mechanical testing was conducted on a United Testing System SFM-20 test fixture.

2.6.2 FLEXURE TESTING. Flexure testing (ASTM D790-76) was performed on 12 ply unidirectional laminates with the fibers oriented at 0° and 90° to the support span. Specimens were 25 mm wide, nominally 100 mm long and tested at a span-to-thickness ratio of 32 to 1. The specimens were three point loaded and the rate of strain in the outer fibers was kept constant at 0.01 (mm/mm)/min. The deflection was measured with a deflectometer for determination of stress versus strain curves and the modulus.



2.6.3 TENSILE TESTING. Tensile testing (ASTM D3039) of 0° and 90° specimens was performed on 18 and 12 ply unidirectional laminates, respectively. 0° tensile specimens were 12.5 mm wide, 225 mm long with a 150 mm gage section. Crossply epoxy/glass tab material was attached to the ends of the specimens with D.E.R. 383/DACH and cured at 40 °C for 4 hours. 90° tensile specimens were 25.4 mm wide, 165 mm long with a 90 mm gage section and tabbed in the same manner as the 0° specimens. Testing was done at a constant crosshead strain rate of 0.5 %/min.

2.7 FRACTOGRAPHY

Scanning electron microscopy (SEM) provided high magnification photomicrographs of the composite failure surfaces. The failed composite specimens required trimming, mounting and coating before they were suitable for examination. The short beam shear specimens were cut through the thickness along the line where the load was applied which allowed a section to come free that displayed the failure surface. The section was mounted on a stub with conductive sliver paste and sputter coated with gold to minimize charging effects from the electron beam. Flexure and tensile specimens were trimmed to approximately 25mm x 25mm, mounted on stubs and gold coated. Prior to coating, delaminated material was removed, when necessary, to reveal the failure surface on the tensile side of flexure specimens.

CHAPTER 3

RESULTS and DISCUSSION

3.1 INTRODUCTION

The interphase of a glass fiber-reinforced epoxy composite was characterized and its effect on composite mechanical properties was measured. Mechanical properties of epoxy/sizing system blends were measured to provide some indication of the properties of the interphase. Both fiber-matrix interphase sensitive mechanical tests (short beam shear, 90° flexure, 90° tension) and interphase insensitive tests (0° flexure, 0° tension) were conducted on high volume composite samples fabricated from the same materials to determine if the interphase and its properties altered the composite mechanical properties and in what manner.

3.2 EFFECT OF THE SIZING ON FIBER TENSILE STRENGTH

Both the test gage length and the presence of the commercial sizing system had an effect on the fiber tensile strength. The dependence of tensile strength on gage length of E-glass fibers is known,^{28,29,30,31,32} however, the effect of a sizing system on strength is not so well characterized.^{30,32} The effect of gage length on tensile strength for brittle fibers (e.g. glass, boron, graphite) is to increase the strength with decreasing gage length. The rate of increase is not uniform, decreasing below a certain gage length. In

glass fibers this transition occurs at a gage length of about 1 to 2 cm.²⁸ This is thought to occur as the result of the presence of two types of flaws, internal and surface, along the fiber. Internal flaws are produced during manufacture of the fibers and limit the ultimate strength of the fibers. Internal flaws include: bubbles, inclusions and other defects. Surface flaws are created after manufacture as the result of damage during handling and processing. The failure of a fiber will occur at the "weakest link" present in the gage length. The "weakest link" is the flaw of greatest severity with internal flaws usually considered less severe than surface flaws.³⁰ The probability of capturing a surface flaw in the gage length is dependent upon the spacing between the flaws. A large gage length will include more surface flaws and reduce the average strength of the fiber at that gage length. Hence the observed increase in the average strength as the gage length decreases. **Figure 10** is a plot of the mean fiber tensile strength versus gage length determined for the bare and sized E-glass fibers used in this study.

A two-sided Student's t analysis indicates that the differences between the fiber types and gage lengths is significant at the 99% level of confidence. The effect of the sizing system probably occurs through protection of the fiber surface. The sizing is applied immediately after manufacture, before the fibers come in contact with one another. The bare fibers were treated with deionized water only. The increase in mean fiber strength is about 12% at all gage lengths for the sized fibers. This increase is similar to that found for E-glass fibers coated with a silane coupling agent alone (12% versus bare fibers) or a model sizing agent (polyvinylacetate) alone (7% versus bare fibers). The silane coupling agent in combination with the polyvinylacetate produced an increase intermediate of either agent used by itself (8% versus bare fibers).³⁰

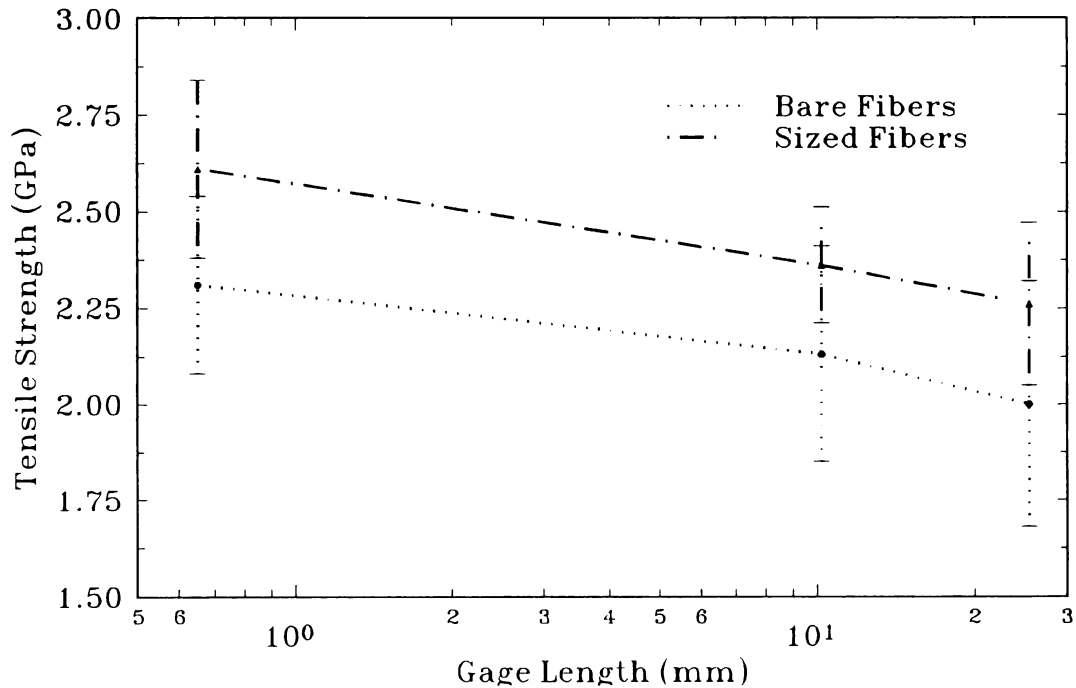


Figure 10. E-Glass Fiber Strength Versus Gage Length

3.3 BLEND PHYSICAL PROPERTIES

3.3.1 GLASS TRANSITION TEMPERATURE. Dynamic Mechanical Analysis provides information on the thermomechanical properties of the epoxy/sizing system blends as a function of temperature. The T_g of a polymer is qualitatively the point at which it undergoes a transition from the glassy state to the rubbery state. For purposes of comparison, the T_g is taken to occur at the inflection point in a plot of the storage modulus (E') versus temperature. **Figure 11** is a plot of T_g determined in this manner versus the amount of epoxy-compatible size added to the stoichiometric mixture of D.E.R. 383/DACH on a weight percent basis.

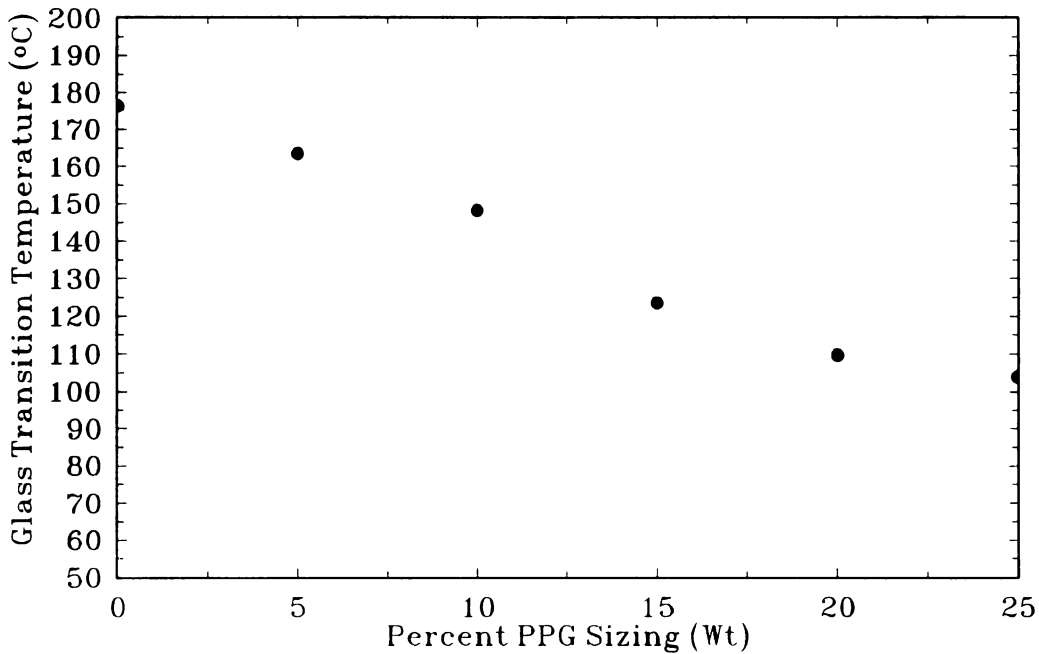


Figure 11. T_g Versus Sizing System Concentration in D.E.R. 383/DACH

It is clear that the polymer created by the addition of the commercial size exhibits a monotonic decrease in the T_g . This indicates that the silane coupling agent and other ingredients in the sizing system are acting to reduce the crosslink density of these mixtures.³³ The silane coupling agent present in commercial sizing systems usually contains a monofunctional chemical group which is reactive with the matrix constituents and can terminate network growth.

3.3.2 MECHANICAL PROPERTIES. The tensile properties of the blends: Young's modulus, Poisson's ratio and tensile strength were determined via mechanical testing. The storage and 0% tangent Young's modulus determined via DMA or by standard ASTM tensile coupon and extensometer methods, respectively, were relatively the same. Toughness, a measure of the material's ability to absorb energy before fracturing was

calculated by integrating the area under the stress versus strain curve.³⁴ **Table 5** lists the values of Young's modulus (E), storage modulus at 25 °C (E'), tensile strength (σ), crosshead failure strain (ϵ), toughness and Poisson's ratio (ν) for the blends.

Table 5. Mechanical Properties of D.E.R. 383/DACH/Sizing Blends

Sizing Concentration (wt %)	Young's Modulus E (GPa)	Storage Modulus E' (GPa)	Tensile Strength σ (MPa)	Failure Strain ϵ (%)	Toughness (MPa)	Poisson Ratio (ν)
0	3.09 ± 0.17	3.46 ± 0.02	72.9 ± 5.0	4.11 ± 0.40	1.58 ± 0.34	0.41 ± 0.03
5	3.38 ± 0.04	3.30 ± 0.02	71.8 ± 0.7	3.39 ± 0.05	1.19 ± 0.20	0.45 ± 0.01
10	3.69 ± 0.06	3.39 ± 0.04	73.4 ± 5.2	3.25 ± 0.35	1.16 ± 0.22	0.45 ± 0.01
15	3.71 ± 0.10	3.62 ± 0.06	72.3 ± 7.3	3.39 ± 0.29	1.25 ± 0.28	0.43 ± 0.01
20	4.01 ± 0.07	3.76 ± 0.03	78.0 ± 4.8	3.33 ± 0.61	1.19 ± 0.21	0.44 ± 0.01
25	3.97 ± 0.12	3.82 ± 0.09	81.6 ± 3.5	3.39 ± 0.28	1.36 ± 0.12	0.45 ± 0.02

Considering the neat D.E.R. 383/DACH as representative of bulk matrix properties, it is apparent that adding the sizing system has significant effects on the properties of the matrix in the interphase region. For comparison, **Figure 12** presents the Young's modulus, tensile strength and toughness versus weight percent sizing added to the stoichiometric D.E.R. 383/DACH.

The Young's modulus and tensile strength increase while the toughness decreases with increasing sizing content. Since all samples were prepared in an identical manner,

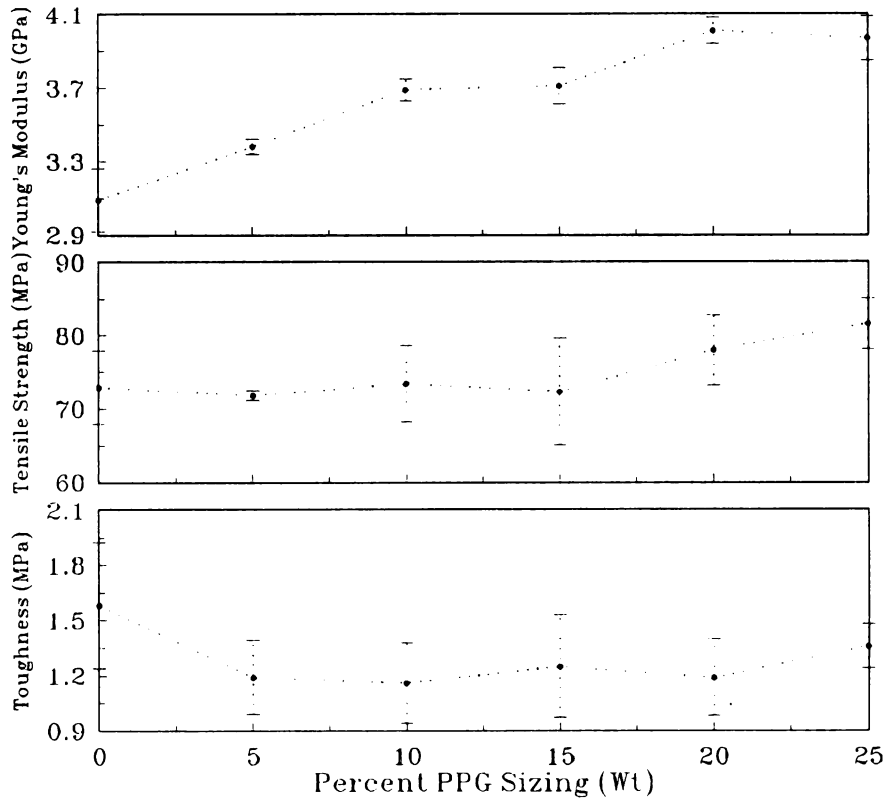


Figure 12. Blend Physical Properties Versus Sizing Concentration

the results must reflect changes in the material properties although the fracture properties are certainly sensitive to flaws. This may be a similar phenomenon³⁵ to that reported previously in which difunctional additives with differing reactivities when added to an epoxy matrix produced increases in tensile strength. Taking the 25% sizing blend as a model for the interphase near the fiber surface, this material would have a lower T_g than the bulk by about 70°C (176°C vs. 100°C). The Young's modulus and tensile strength of the interphase would be increased by 28 and 12% respectively versus the bulk matrix. The failure strain and toughness would decrease by 18 and 14% respectively. Overall, the interphase created by the commercial sizing system and the matrix would be



characterized as a stiffer, stronger, lower toughness interphase.

These results suggest that the interphase formed when the sized fiber is brought into contact with the matrix during formation of the composite can have significantly different mechanical properties than the bulk matrix. In an actual composite, the solubility of the sizing system and matrix components would determine the extent of the interaction and the resultant composition. There would undoubtedly be a gradient of properties where the interphase material near the fiber surface would have a high concentration of sizing and low bulk matrix. As the distance from the fiber surface increases, the sizing content decreases until the bulk matrix properties are reached at some distance away from the fiber surface. Currently there is no acceptable method for quantitatively determining this gradient and distribution in a real interphase, the values obtained here serve to provide some limits that "bracket" the expected material behavior of the fiber-matrix interphase.

3.4 EFFECT OF THE SIZING ON INTERFACIAL BEHAVIOR

3.4.1 FIBER-MATRIX FAILURE LOCUS. Embedded single fiber and ITS tests provide insight into how modification of the interphase by the sizing system affect fiber-matrix failure modes and adhesion. **Figure 13** is a polarized transmitted light photomicrograph of a typical fiber break in a D.E.R. 383/DACH/Bare E-glass embedded single fiber coupon. The specimen was strained in a direction parallel to the fiber axis until the fiber started to fracture in the coupon. The photomicrograph shows the region around the break taken immediately after the fiber fractured. A small matrix

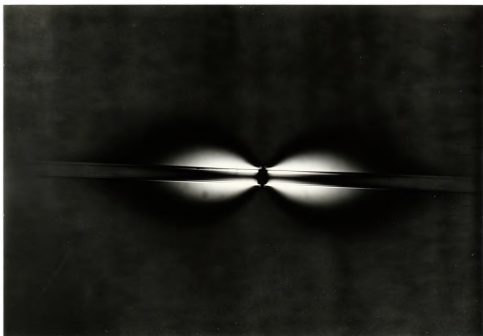


Figure 13. Fiber Break at Low Strain, D.E.R. 383/DACH/Bare E-Glass, X67

crack extends outward from the fiber into the matrix. The light regions extending approximately 3 fiber diameters into the matrix are photoelastic stress birefringence patterns. The stress birefringence patterns qualitatively correspond to a decreasing stress gradient away from the fiber. As the coupon was strained further, the nature of the fiber-matrix failure changed. **Figure 14** is a photomicrograph of a fiber break in polarized light. The matrix crack has not extended appreciably, however there are changes at the fiber-matrix interface. An interfacial crack has appeared at the fiber break and extends down both sides of the break for about 3 fiber diameters. The breadth of the birefringence patterns has decreased to less than 2 fiber diameters and the photoelastic area extends down the length of the fragment away from the break, indicating a more uniform stress state along the fiber. The fiber-matrix failure mode



changes from matrix cracking to fiber-matrix interfacial debonding at the fiber break. The arresting of the matrix crack by the bulk matrix away from the fiber surface has shifted the failure locus to the fiber-matrix interface.

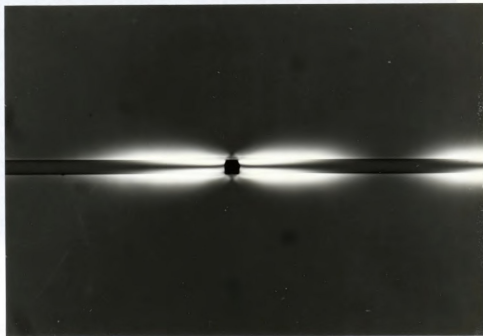


Figure 14. Fiber Break at High Strain, D.E.R. 383/DACH/Bare E-Glass, X67

This is not the behavior observed in D.E.R. 383/DACH and other epoxy systems³⁶ when the epoxy-compatible sizing agent is present in the fiber-matrix interphase. **Figure 15** is a photomicrograph of a typical fiber break in this system using polarized transmitted light. The initial matrix crack is larger than that observed in the bare E-glass system, in this case extending on both sides of the fiber and forming a penny shaped crack if viewed end-on. There is no debonding at the fiber-matrix interface. The birefringence pattern includes two bright regions at the tip of the crack, indicating a high level of stress. At this level of strain there are very few fiber breaks



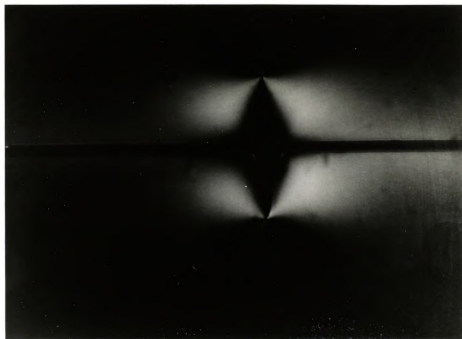


Figure 15. Fiber Break at Low Strain, D.E.R. 383/DACH/Sized E-Glass, X67

in the coupon, three on average. When the specimens were strained past the point where these initial cracks appeared, the coupon failed due to continued matrix crack propagation perpendicular to the fiber axis. These results indicate that modification of the interphase by the sizing system changes the failure mode. Instead of additional strain energy being absorbed by interfacial debonding, as in the bare E-glass system, the matrix crack propagates and results in the failure of the coupon. Recalling the epoxy/sizing system blend data, the interphase could be reasonably expected to be lower in toughness, leading to larger matrix cracks under the same stress concentration at the broken fiber end. Once these cracks exceed critical flaw size the test coupons fail catastrophically.



3.4.2 FIBER-MATRIX ADHESION. Embedded single fiber and ITS testing were used to measure the level of fiber-matrix adhesion in model and actual composites. Embedded single fiber results were obtained for bare E-glass fibers only, failure of the test coupons containing sized fibers occurred after the very first breaks in the coupons. The fiber tensile strength results were extrapolated to the critical length, l_c , to determine the interfacial shear strength. **Table 6** lists the values measured for the distribution of fragment lengths and the interfacial shear strength calculated for a fiber tensile strength of 2.34 GPa at l_c .

Table 6. Embedded Single Fiber Results for D.E.R. 383/DACH/Bare E-Glass

Number of Fragments	Weibull α	Weibull β	l_c (μm)	Interfacial Shear Strength (MPa)
294	3.23	28.2	376	54.7

This value of interfacial shear strength is similar to that measured in an epoxy/polyamide system with bare E-glass fibers of 58.1 MPa.³²

The Interfacial Testing System (ITS) provides comparative data on the interfacial shear strengths of the bare and sized E-glass fibers in actual composites. A value of 76 GPa³⁷ was used for the tensile modulus of E-glass fibers and the shear modulus of D.E.R. 383/DACH was measured as 1.10 GPa. **Table 7** lists the mean interfacial shear strength, standard deviation and number of fiber ends tested for the two fiber types.



Table 7. ITS Results for D.E.R. 383/DACH/E-Glass Composites

Fiber Type	Interfacial Shear Strength (MPa)	Standard Deviation (MPa)	Number of Fibers Tested
Bare	44.6	3.0	30
Sized	60.1	3.3	28

The interfacial shear strength (IFSS) increased 35% for the sized fibers versus the bare. A two-sided Student's t-test indicates that the difference is significant at the 99% level of confidence. These results indicate that the application of the sizing and the consequent formation of the interphase increased the level of fiber-matrix adhesion. It could reasonably be expected that under the multi-axial state of stress at the fiber-matrix interphase, stronger fiber-matrix adhesion would reduce the tendency to grow an interfacial crack thereby placing more energy into driving the matrix crack.

The increase in interfacial shear strength is consistent with theoretical mechanical models of fiber-matrix adhesion. Rosen³⁸, Cox³⁹, Whitney and Drzal⁴⁰ have shown that the square root of the shear modulus of the matrix appears explicitly in any model of the interfacial shear strength. It has been demonstrated experimentally^{41,42} that the fiber-matrix interfacial shear strength has a dependence on both the product of the strain-to-failure of the matrix times the square root of the shear modulus as well as on the difference between the test temperature and T_g when the interfacial chemistry is held constant.



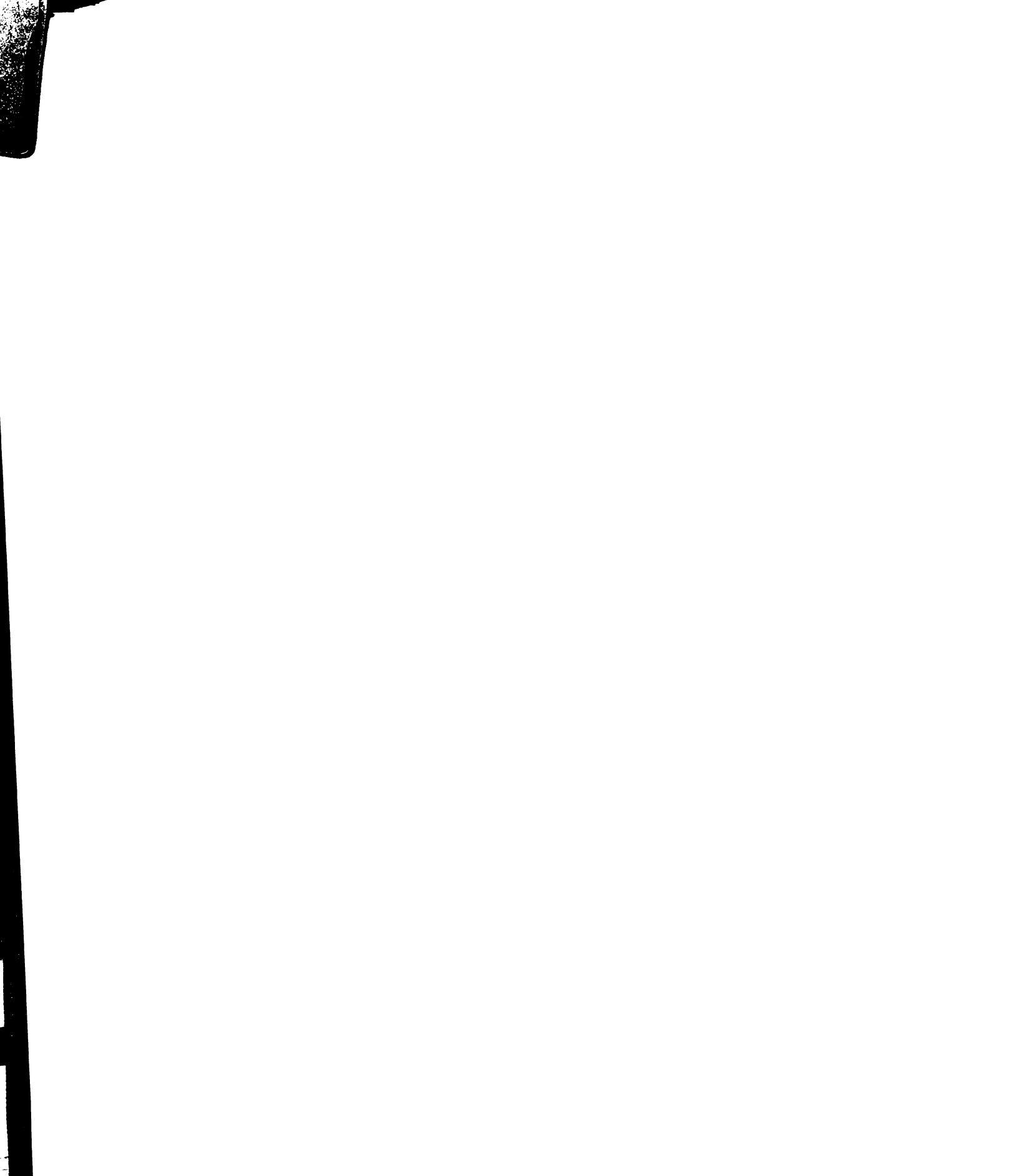
3.5 EFFECT OF THE SIZING ON COMPOSITE PROPERTIES

3.5.1 SHORT BEAM SHEAR. Short beam tests provided information on the apparent interlaminar shear strength (ILSS) of laminates made with bare and sized E-glass fibers. In all cases the specimens failed in shear at or near the midplane, allowing comparisons to be made between fiber types. The ILSS, standard deviation and number of specimens tested are given in **Table 8**.

Table 8. SBS Results for D.E.R 383/DACH/E-Glass Laminates

Fiber Type	Apparent Interlaminar Shear Strength (MPa)	Standard Deviation (MPa)	Number of Specimens Tested
Bare	71.3	1.6	9
Sized	80.2	2.2	12

The increase in the apparent ILSS for the sized versus bare fibers is 12.4%, approximately 50% of the increase observed in the interfacial shear strength as measured by ITS testing. The apparent ILSS is certainly sensitive to the macroscopic properties of the laminates, but changes in fiber-matrix adhesion and interphase properties are expected to influence the results. Recalling that the fiber and void volume fractions are similar for the SBS specimens, direct comparison between fiber types can be made. The apparent ILSS values of unidirectional composites have been found to rank with fiber-matrix bond strengths,^{25,43} however, changes in the apparent ILSS were not found to be proportional with changes in fiber-matrix adhesion. The short beam shear test will be sensitive to macroscopic strength limiting defects such as voids and fiber misalignments



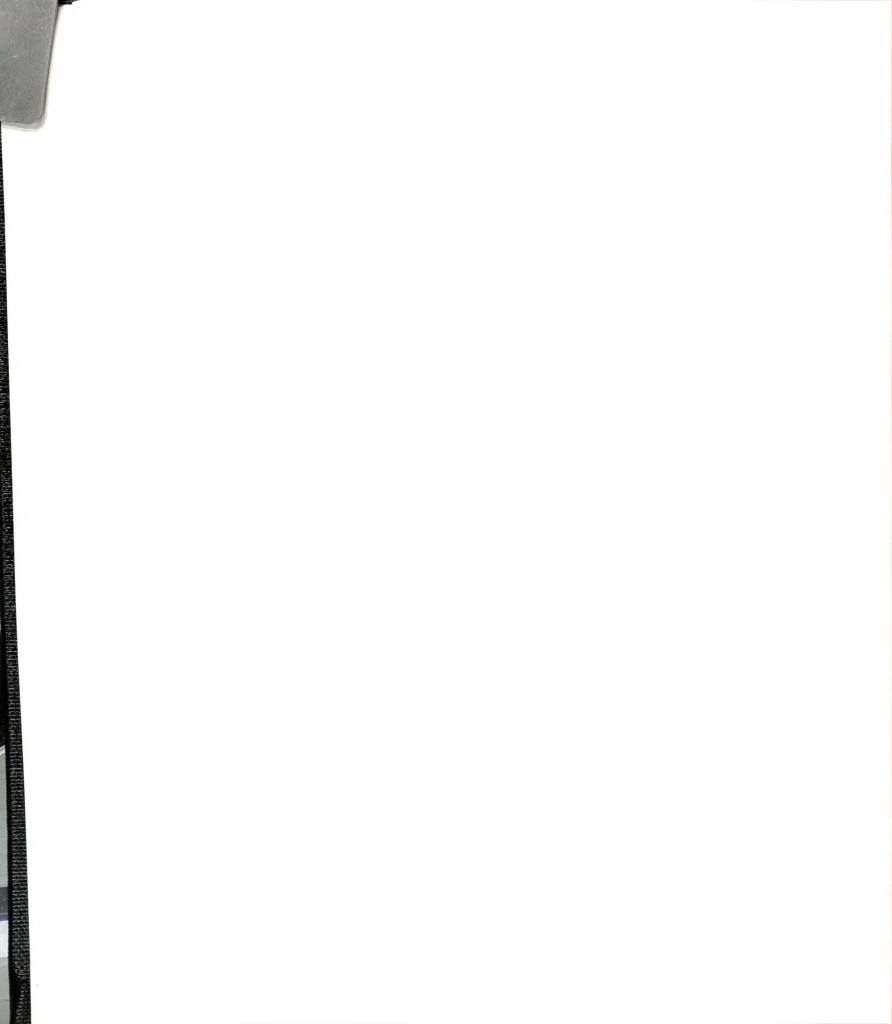
that do not affect ITS results. Recalling the lower toughness of the model interphase blends, the increase in adhesion at the interface may be partially offset by a decrease in the toughness of the interphase. An interphase lower in toughness would provide a path of lesser resistance for the propagation of defect-initiated intralaminar failure.

3.5.2 90° FLEXURE. The 90° flexural properties were determined using the procedure described above. **Table 9** lists the properties measured for laminates with bare and sized E-glass fibers. The flexural modulus was not affected by the fiber type. The amount of sizing applied to the fibers is too small to increase the modulus of the bulk matrix away from the fiber and affect the result between fiber types.

Table 9. 90° Flexural Properties of D.E.R. 383/DACH/E-Glass Laminates

Fiber Type	90° Flexural Strength (MPa)	90° Flexural Strain at Failure (%)	90° Flexural Modulus (GPa)	Number of Specimens Tested
Bare	75.6 ± 1.8	0.48 ± 0.01	15.7 ± 0.26	5
Sized	102 ± 5.2	0.69 ± 0.05	15.6 ± 0.23	5

In the 90° direction, the fiber-matrix interphase is a controlling factor in the flexural strength. Failure of the test specimens occurred on the tensile surface, forming a hinge crack that did not extend through the specimen. Here a 35% increase in flexural strength is measured in direct proportion to the increase in interfacial shear strength measured with the ITS tests. This indicates an increase in the transverse tensile strength of the fiber-matrix interphase. Apparently the lower toughness of the interphase and its tendency to create matrix cracks and not debond under shear loading does not affect the



interphase when it is loaded in transverse tension. An increase in the strain to failure of the sized versus bare fiber laminates is not paralleled by the results of the model interphase. Increased fiber-matrix adhesion would limit the formation of fiber-matrix interfacial cracks that would lead to premature failure of the specimens and thereby increase the strain to failure.

3.5.3 0° FLEXURE. Flexural properties in the 0° direction are largely determined by the fiber properties; however, the matrix or interphase may control the failure mode or path which may in turn affect the strength of the composite. The 0° flexural properties of the composites made with bare and sized E-glass are listed in **Table 10**.

Table 10. 0° Flexural Properties of D.E.R. 383/DACH/E-Glass Laminates

Fiber Type	0° Flexural Strength (MPa)	0° Flexural Strain at Failure (%)	0° Flexural Modulus (GPa)	Number of Specimens Tested
Bare	1010 ± 60	3.0 ± 0.2	39.5 ± 1.3	6
Sized	1260 ± 50	3.5 ± 0.2	44.2 ± 3.3	6

Laminates with either bare or sized E-glass fibers failed first on the tensile surface of the test specimen but the nature of the event differed. **Figures 16 and 17** are photographs of the tensile surfaces and edges of failed test coupons that were fabricated with bare E-glass. **Figure 16** illustrates the breakage of fiber bundles which then propagated delaminations along the tensile surface of the specimen. This process occurred over the last 10 to 15 seconds of the test, and failure occurred gradually rather than catastrophically. The lack of penetration of the failure zone into the interior of the



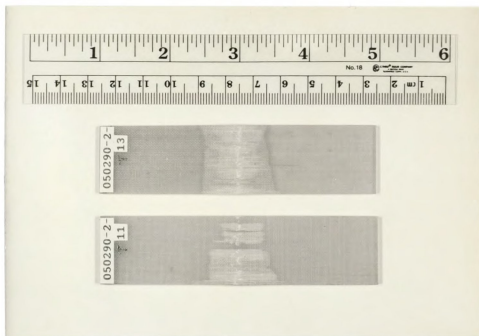


Figure 16. 0° Flexure Specimens, Tensile Side, D.E.R. 383/DACH/Bare E-Glass

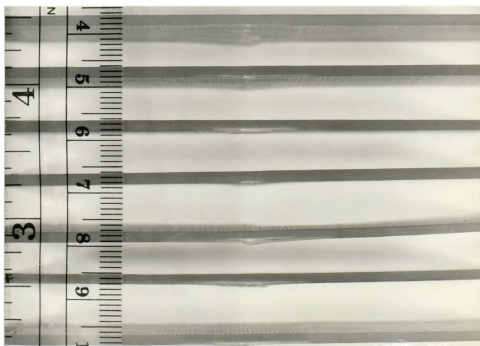


Figure 17. 0° Flexure Specimens, Edge View, D.E.R. 383/DACH/Bare E-Glass

specimens, **Figure 17**, indicates that strain energy was being absorbed by delamination rather than the growth of matrix cracks into the specimen.

The failure behavior of the laminates made with sized E-glass fibers was different. **Figures 18 and 19** are photographs of the tensile surfaces and edges of failed specimens. The specimens failed catastrophically through the thickness, and the delaminations shown in **Figure 18** occurred during the failure, not before. Regions of tensile failure (fiber pull-out) and compressive failure (crushing) can be seen in **Figure 19**. The change in failure at the single fiber level as shown by the embedded single fiber test is mirrored by the failure behavior at the macroscopic level.

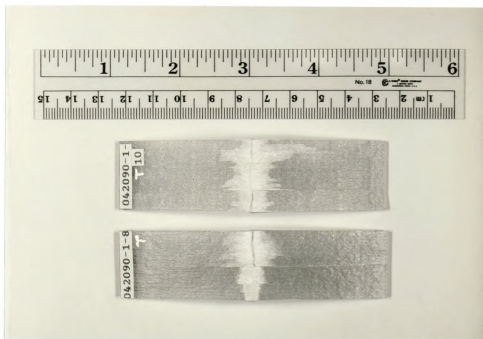
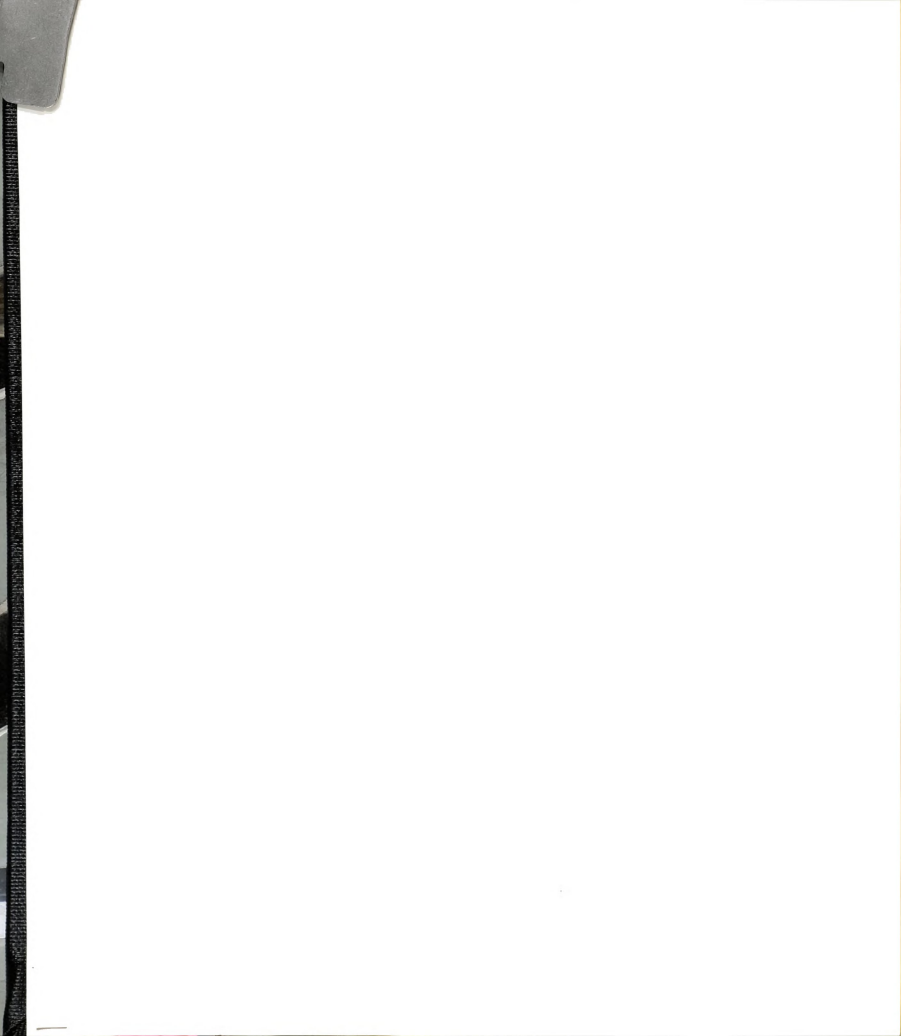


Figure 18. 0° Flexure Specimens, Tensile Side, D.E.R. 383/DACH/Sized E-Glass



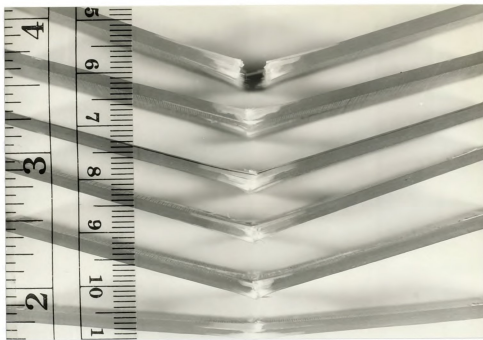


Figure 19. 0° Flexure Specimens, Edge View, D.E.R. 383/DACH/Sized E-Glass

The increase in the 0° flexural strength is 25% for the sized versus bare fiber laminates. This can be partially attributed to the measured 12% increase in the tensile strength of sized versus bare fibers. Reduction of the 0° flexural strength of the sized fiber to account for the increase in fiber strength yields a value of 1,121 MPa. The difference between the bare and sized fiber laminate 0° flexural strength is reduced to 11%. The contribution of the fiber tensile strength difference may be lost during production of the laminates, so the increase in 0° flexural strength due to the sizing system is likely between 11 and 25%. The change in failure mode from delamination to through-the-thickness failure indicates that the arresting of delaminations is an important modification afforded by the use of a sizing system. The increase of the strain at failure of sized versus bare fiber laminates is the result of the increase in strength.



3.5.4 90° TENSILE. Differences in the 90° tensile properties of laminates made with bare and sized E-glass fibers were noted, however, quantifying these differences was made difficult by specimen failure at or in the grips. **Table 11** lists the 90° tensile strength and crosshead strain at failure and modulus.

Table 11. 90° Tensile Properties of D.E.R. 383/DACH/E-Glass Laminates

Fiber Type	90° Tensile Strength (MPa)	90° Tensile Strain at Failure (%)	Tangent Modulus of Elasticity (GPa)	Number of Specimens Tested
Bare	23.5 ± 2.2	1.1 ± 0.2	1.92 ± .10	6
Sized	37.0 ± 4.8	2.1 ± 0.2	2.06 ± .18	6

If the stress concentrations due to the tabs and grips is taken to be constant between all specimens, then these values can still be used for comparisons between fiber types. The increase in 90° tensile strength corresponds to the change in the level of fiber-matrix adhesion measured via ITS testing. The complex state of stress introduced by the grips makes the difference in strength impossible to explain in terms of loading at the single fiber level. No effect on the modulus of the laminates was noted, the amount of sizing system introduced into the interphase is too small to effect the bulk matrix properties. No differences in the macroscopic failure mode was noted between the bare and sized fiber specimens.

3.5.5 0° TENSILE. Specimen failure at or in the grips also occurred for the 0° tensile specimens. **Table 12** lists the properties determined for the bare and sized fiber laminates.

Table 12. 0° Tensile Properties of D.E.R. 383/DACH/E-Glass Laminates

Fiber Type	0° Tensile Strength (MPa)	0° Tensile Strain at Failure (%)	Tangent Modulus of Elasticity (GPa)	Number of Specimens Tested
Bare	580 ± 33	6.2 ± 0.3	11.5 ± 0.5	4
Sized	944 ± 28	9.2 ± 0.4	11.8 ± 0.1	5

If the stress concentration due to the tabs and grips is taken to be constant between all specimens, then these values can still be used for comparison between fiber types. The properties in the 0° direction are expected to be fiber dominated, as is the case for the modulus. However, the increase in the strength is greater than the single fiber tensile strength increase for bare versus sized fibers of 12%. The complex stress state in the grips may introduce fiber-matrix interfacial cracks that reduce the bare fiber laminate strength. No change in the macroscopic failure behavior between fiber types was observed. The increase in failure strain is a result of the increase in laminate strength.

3.6 EFFECT OF THE SIZING SYSTEM ON COMPOSITE FRACTOGRAPHY

3.6.1 SHORT BEAM SHEAR. Differences in the microscopic failure surfaces of bare and sized fiber short beam shear specimens were noted. A scanning electron microscope (SEM) was used to examine the failure surfaces of specimens prepared as discussed in Chapter 2. **Figure 20** is a SEM photomicrograph at X1,000 of a SBS coupon made with bare fibers. The surfaces of the fibers are smooth and appear free of matrix. The lack of matrix adhering to the fibers is interpreted as an indication of a weak

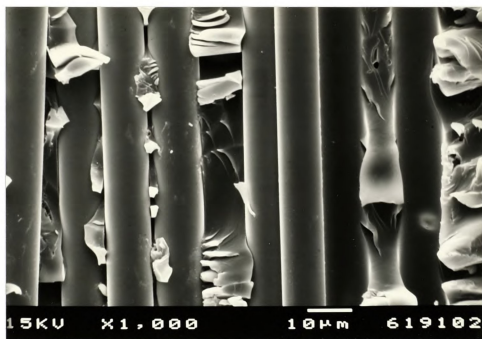


Figure 20. SBS Failure Surface, D.E.R. 383/DACH/Bare E-Glass

fiber-matrix interface.⁴⁴ The macroscopic failure of the specimen was interlaminar, confined to a plane between plies. SEM examination revealed that the failure on the microscopic level was also contained to a plane and no broken fibers were observed. This indicates that the failure occurred in pure shear, corroborated by experiments designed to load the interface in pure shear or mixed modes⁴⁵ in glass/epoxy composites. The macroscopic failure of the SBS specimens with sized fibers was the same as the bare fiber specimens. **Figure 21** is a SEM photomicrograph of the failure surface of a sized fiber SBS specimen. There is a layer of matrix adhering to the fibers which is a qualitative sign of good fiber-matrix adhesion.⁴⁶ The planar microscopic failure surface and the hackled appearance of the matrix are considered indications of shear failure in the matrix.⁴⁵ The presence of the sizing has increased the

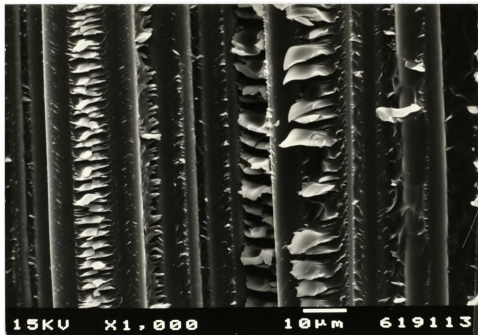
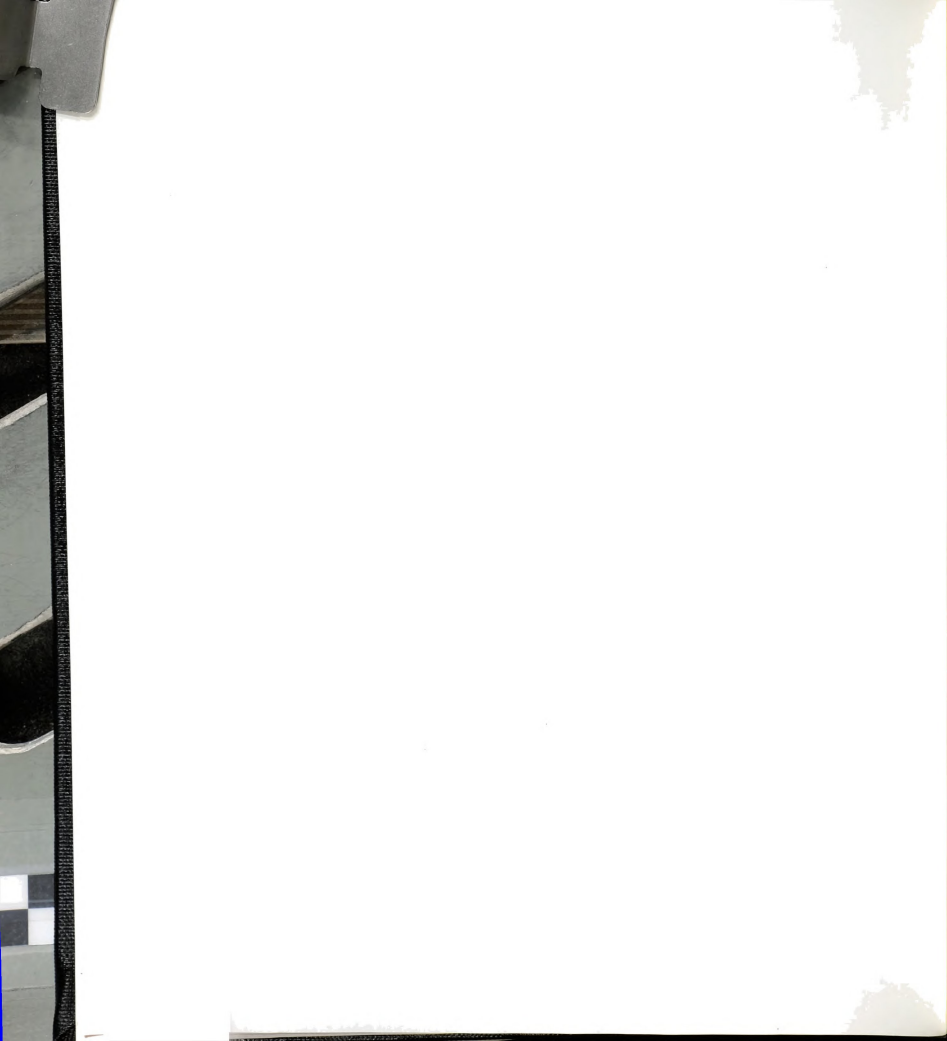


Figure 21. SBS Failure Surface, D.E.R. 383/DACH/Sized E-Glass

fiber-matrix adhesion as characterized by microscopic examination of the failure surfaces and correlates with the increase in fiber-matrix interfacial shear strengths.

3.6.2 0° FLEXURE. The macroscopic failure of 0° flexure specimens made with bare fibers was characterized by delaminations on the tensile surfaces of the coupons. **Figure 22** is a SEM photomicrograph of a representative microscopic failure surface of a bare fiber specimen. The surfaces of the fibers are devoid of matrix, indicating poor adhesion and failure at the fiber-matrix interface. The fact that the delaminations occurred in overlying planes combined with the appearance of the matrix indicate a mixed failure mode of shear + tension.⁴⁵ The macroscopic failure of 0° flexure specimens made with sized fibers was through the thickness,



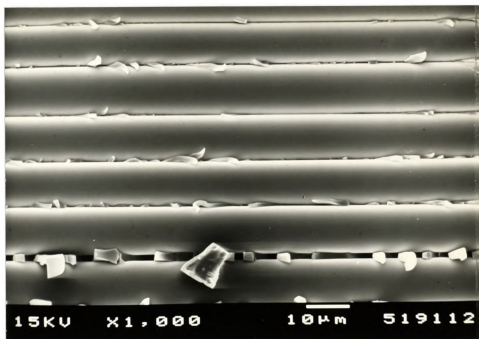


Figure 22. 0° Flexure Failure Surface, D.E.R. 383/DACH/Bare E-Glass

regions of fiber pull-out and crushing could be observed. **Figure 23** is a X35 SEM photomicrograph of a section through the thickness of a failed specimen. The neutral axis runs from A to B, above this line the specimen failed in tension (fiber pull-out), below this line compression. **Figure 24** is a X1,000 view of fiber surfaces on the compressive side. The appearance of the matrix adhering to the fibers is characteristic of mixed mode shear + compressive failure at the surface.⁴⁵ Fibers on the tensile side of the neutral axis are shown in **Figure 25**. The fibers are covered with a layer of matrix, indicating increased adhesion between the fiber and matrix and a shift in the failure locus to the interphase. The pull-outs combined with the appearance of the matrix are characteristic of mixed mode shear + tensile failure at the surface.⁴⁵ Inspection of the failure surfaces of bare and sized fiber 0° flexural specimens has revealed qualitative



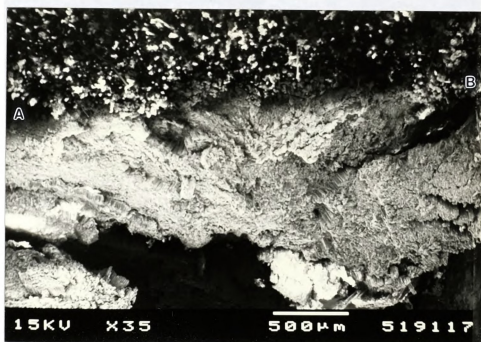


Figure 23. 0° Flexure Failure Surface, D.E.R. 383/DACH/Sized E-Glass

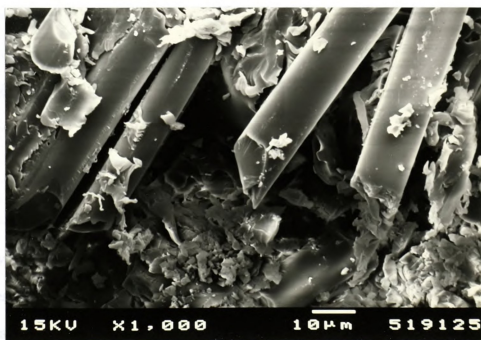
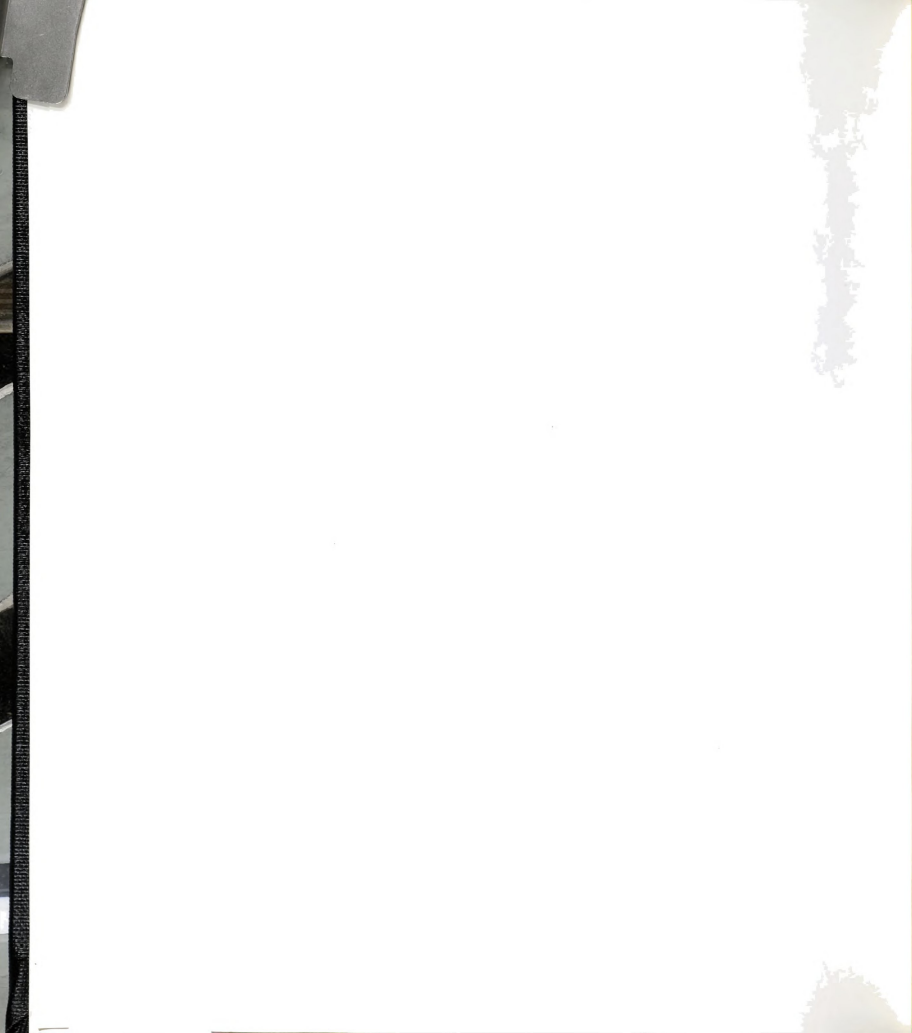


Figure 24. 0° Flexure Failure Surface, Compressive Side, D.E.R. 383/DACH/Sized E-Glass



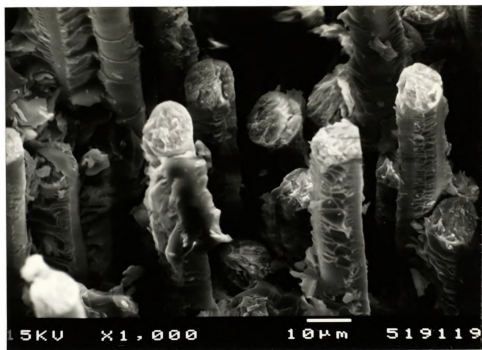


Figure 25. 0° Flexure Failure Surface, Tensile Side, D.E.R. 383/DACH/Sized E-Glass

increases of the adhesion between fiber and matrix of sized fiber specimens. The failure locus shifted from the fiber-matrix interface to the interphase for both mixed mode loading conditions of shear + tension and shear + compression for the sized fiber specimens.

3.6.3 90° TENSILE. The failure of the 90° tensile specimens was influenced by the stress state introduced when the failure occurred at or in the grips. The complex stress state was revealed in SEM photomicrographs of both the bare and sized specimens. **Figures 26 and 27** are SEM photomicrographs at X1,000 of 90° tensile specimens made with bare and sized fibers, respectively. The specimen made with bare fibers has very little matrix adhering to the fibers, again indicating poor fiber-matrix adhesion. The

1951

1952

1953

1954

1955

1956

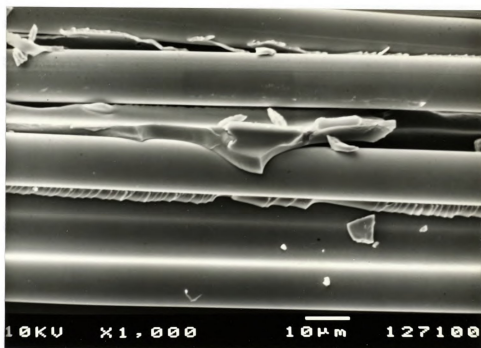


Figure 26. 90° Tensile Failure Surface, D.E.R. 383/DACH/Bare E-Glass

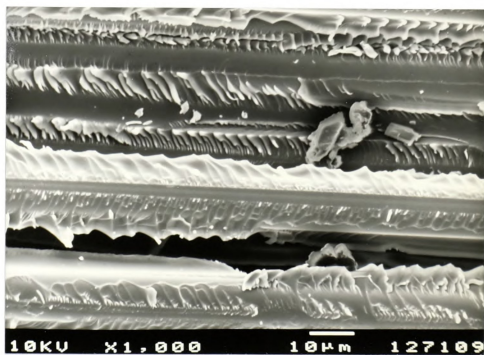


Figure 27. 90° Tensile Failure Surface, D.E.R. 383/DACH/Sized E-Glass



failure surface is not confined to a plane and the matrix in this region has widely spaced hackles. This indicates that this surface failed both in tension, as expected from the loading, and shear, possibly introduced by the grips. The specimen made with sized fibers has matrix adhering to the fibers, indicating an increase in adhesion and a shift in the failure from the interface to the interphase. The non-planar failure surface and hackled matrix again indicate a mixed mode of failure of tension + shear.

3.6.4 0° TENSILE. The failure of the 0° tensile specimens also occurred at or near the grips. **Figures 28 and 29** are SEM photomicrographs at X1,000 of the failure surfaces of specimens made with bare and sized fibers, respectively. The bare fiber specimen has clean fiber pull-outs, again indicative of poor fiber-matrix adhesion. The failure path traveled along the fiber-matrix interface, similar to the behavior observed in the embedded single fiber test. Sized fiber specimens also reflected the behavior observed in the embedded single fiber test; the failure surface is relatively smooth with blocks of fiber and matrix at different levels. If the large matrix cracks observed in the single fiber test occurred at fiber breaks in the tensile test coupon, the failure surface would tend to be confined to a plane perpendicular to the fiber's long axis. The level of adhesion and failure behavior at the fiber-matrix interface have again influenced the failure at the microscopic level.

failure surface

friction

loading

flexure test

the failure

method

2.2.4.1

graph

of specimens

cross fiber

removed

concluded

in the timber

flexure and

flexure test

and to

absorption

failure

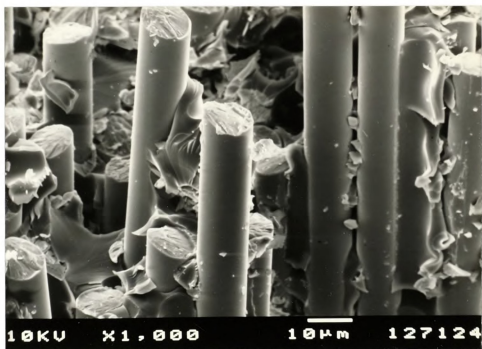


Figure 28. 0° Tensile Failure Surface, D.E.R. 383/DACH/Bare E-Glass

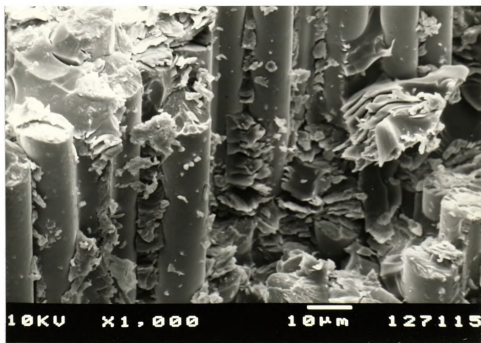


Figure 29. 0° Tensile Failure Surface, D.E.R. 383/DACH/Sized E-Glass

CHAPTER 4

CONCLUSIONS

It has been demonstrated that a sizing system's interaction with the bulk matrix in a glass fiber-reinforced epoxy matrix composite has effects at three levels: molecular, microscopic and macroscopic.

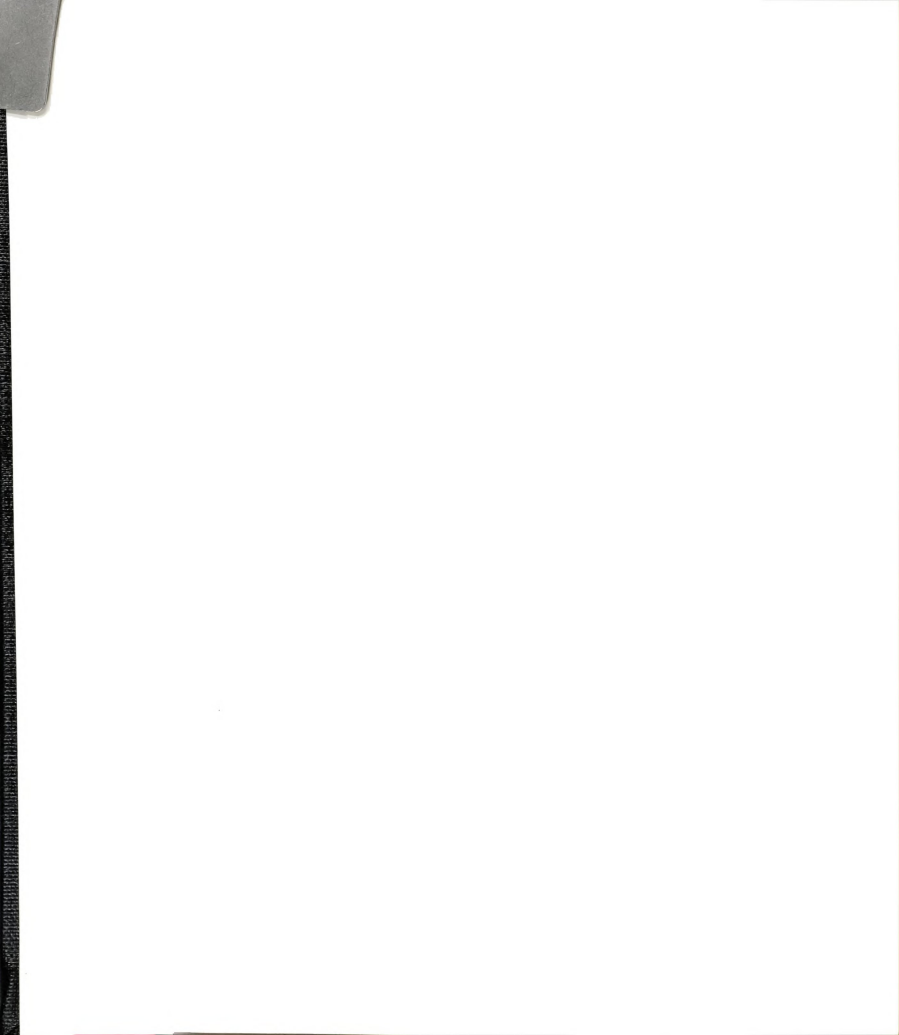
At the molecular level, modelling of the interphase via bulk measurements of epoxy/sizing system blends has shown that the sizing system can significantly alter the physical properties of the interphase. An epoxy blend containing 25% sizing system used to model the interphase exhibited increases in the Young's modulus and tensile strength of 28% and 12% respectively. The toughness of the model interphase was found to decrease by 14%. The T_g of the blend decreased by 72 °C versus the bulk epoxy.

At the microscopic level, embedded single fiber and ITS testing revealed effects of the sizing system on level of fiber-matrix adhesion and failure mode. The presence of the sizing system increased the level of fiber-matrix adhesion by 35% and shifted the locus of failure from interfacial debonding to matrix cracking. The change in adhesion can be attributed to the increased modulus of the sizing system-matrix interphase and chemical bonding through the silane coupling agent. The increased level of adhesion and decreased toughness of the interphase combine to shift the fiber-matrix failure locus.

At the macroscopic scale of composite test specimens, the changes in the



interphase primarily affected the failure behavior of fiber dominated tests (0° flexure, 0° tension) and affected both the failure behavior and mechanical properties of interphase sensitive composite tests (short beam shear, 90° flexure, 90° tension). All interphase sensitive tests measured increases in the strength values and no changes in the moduli. Macroscopic failure of the specimens was identical between bare and sized fiber specimens. Interphase insensitive tests showed effects on the physical properties due to the presence of the sizing system; but the properties were still largely fiber dominated. The macroscopic failure of 0° tensile specimens did not change with fiber type, however, the 0° flexure specimens changed from delamination to through-the-thickness failure. SEM examination of failure surfaces indicated qualitative increases in fiber-matrix adhesion in all stress states, and a shift in the failure path from interfacial to the interphase for the sized fiber specimens.



LIST OF REFERENCES

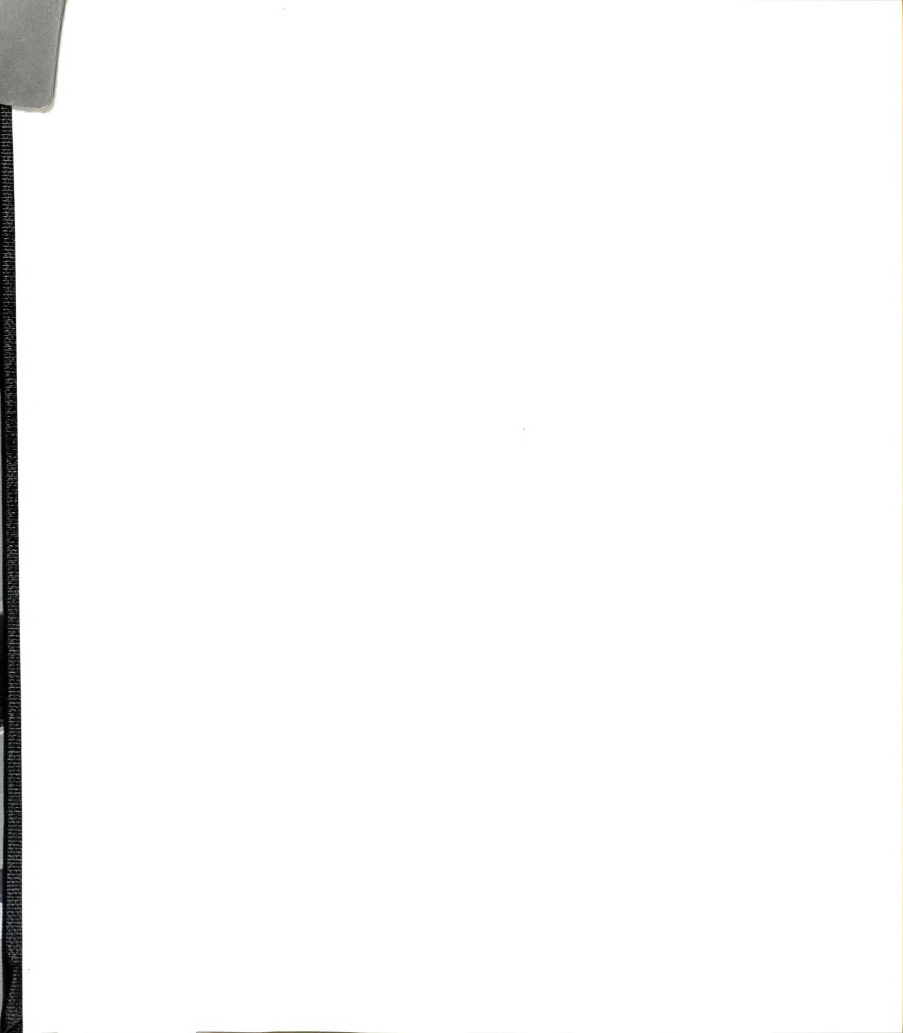


LIST OF REFERENCES

1. E. P. Plueddemann, Silane Coupling Agents, 2nd ed., (New York: Plenum Press, 1990), 86.
2. Ibid., 116.
3. Ibid., 55.
4. Ibid., 35.
5. C. H. Chiang, H. Ishida and J. L. Koenig, J. Colloid Interface Sci. 74 (1980): 396.
6. K. P. Hoh, H. Ishida and J. L. Koenig, Polymer Composites 11, no. 2 (1990): 121.
7. H.-J. Kang, W. Meesiri and F. D. Blum, Materials Science and Engineering A126 (1990): 265.
8. D. J. Pawson and F. R. Jones, in: Controlled Interphases in Composite Materials, ed. H. Ishida (Amsterdam: Elsevier, 1990), 407.
9. Plueddemann, 101.
10. H. Ishida and J. L. Koenig, Journal of Polymer Science: Polymer Physics Edition 17 (1979): 615.
11. H. Ishida, in: Molecular Characterization of Composite Interfaces vol. 27, Polymer Science and Technology, ed. H. Ishida and G. Kumar (New York: Plenum Press), 25.
12. Dow Corning Corporation, A Guide to Dow Corning Silane Coupling Agents (1985), 15.
13. Plueddemann, 87.
14. Ibid., 147.
15. Ibid., chapter 5.



15. Ibid., chapter 5.
16. L. T. Drzal, SAMPE 19 (1983): 7.
17. L. T. Drzal, in: Advances in Polymer Science II vol. 75, ed. K. Dusek (Spring-Verlag: 1985)
18. M. C. Waterbury and L. T. Drzal, J. Reinf. Plast. & Composites 8 (1989): 627.
19. American Society for Testing and Materials, Annual Book of ASTM Standards, vol. 8.01 (Philadelphia: ASTM, 1988), 167.
20. L. T. Drzal, M. J. Rich, J. D. Camping and W. J. Park, Proceedings of the 35th Annual Technical Conference, Reinforced Plastics/Composites Institute, (The Society of the Plastics Industry, Inc.: 1980), 1.
21. L. T. Drzal and P. Herrera-Franco, in: The Engineered Materials Handbook: Adhesives and Sealants vol. 3 (ASM Intl., 1990), 391.
22. A. Kelly, Proc. Royal Soc. A. 319 (1970): 95.
23. A. C. Cohen, Jr., Technometrics (7): 579.
24. D. L. Caldwell, D. A. Babbington and C. F. Johnson, in: Interfacial Phenomena in Composite Materials '89 ed. F. R. Jones (Butterworth, 1989), 44.
25. D. L. Caldwell and F. M. Cortez, Modern Plastics (September 1988): 132.
26. T.-H. Tsiang, Damage Development in Fiber Composites Due to Bearing, ScD Dissertation, M.I.T. (1983).
27. D. H. Grande, Microbonding Test for Measuring Shear Strength of Fiber/Matrix Interface in Composite Materials, M.S. Thesis, M.I.T. (1983).
28. R. A. Larder and C. W. Beadle, J. of Composite Materials 9 (July 1975): 241.
29. C. Zweben, W. S. Smith and M. W. Wardle, Composite Materials: Testing and Design (Fifth Conference) ASTM STP 674, ed. S. W. Tsai (American Society for Testing and Materials, 1979), 228.
30. W. A. Fraser, R. H. Ancker, A. T. DiBenedetto and B. Elbirli, Polymer Composites 4, no.4 (October 1983): 238.
31. K. K. Phani, J. Appl. Phys. 62, no.2 (15 July 1987): 719.
32. A. T. DiBenedetto and P. J. Lex, Polymer Engineering and Science 29, no. 8 (April 1989): 543.



33. E. A. Turi, Thermal Characterization of Polymeric Materials (Academic Press Inc., 1981), 515.
34. R. W. Hertzberg, Deformation and Fracture Mechanics of Engineering Materials (New York: John Wiley & Sons Inc., 1976), 27.
35. A. Garton and G. S. Haldankar, J. Adhesion 29 (1989): 13.
36. A. N. Netravali, P. Schwartz and S. L. Phoenix, Polymer Composites 10 no.6 (1989): 385.
37. D. Hull, An Introduction to Composite Materials (Cambridge: Cambridge University Press, 1987), 14.
38. B. Rosen, in: Fiber Composite Materials chap. 3 (American Society for Metals, 1964), 37.
39. H. L. Cox, Brit. J. Appl. Phys. 3 (March 1952): 72.
40. J. M. Whitney and L. T. Drzal, in: Toughened Composites STP 937 (Philadelphia: American Society for Testing Materials, 1987), 179.
41. V. Rao and L. T. Drzal, Polymer Composites (in press) (1991).
42. L. T. Drzal, Mater. Sci. Eng., Trans ASME A126 (1990): 289.
43. Hull, 48.
44. Ibid., 54.
45. A. Voloshin and L. Arcan, J. of Composite Materials (July 1979): 240.
46. Hull, 55.





MICHIGAN STATE UNIV. LIBRARIES



31293009093471